American Mineralogist, Volume 106, pages 1873–1889, 2021

Contrasting magma compositions between Cu and Au mineralized granodiorite intrusions in the Tongling ore district in South China using apatite chemical composition and Sr-Nd isotopes

Li-Chuan Pan[1], Rui-Zhong Hu[1,2,*,†], Abiola Oyebamiji[1], Hong-Yuan Wu[3], Jin-Wei Li[1], and Jin-Xiang Li[1]

[1]State Key Laboratory of Ore Deposit Geochemistry, Institute of Geochemistry, Chinese Academy of Sciences, Guiyang 550081, China
[2]College of Earth and Planetary Sciences, University of Chinese Academy of Sciences, Beijing 100049, China
[3]The Bureau of Geology and 321 Mineral Exploration Team of Anhui Province, Tongling 244000, China

Abstract

Identifying magma fertility is an important task in ore genesis research. In this paper, we use apatite chemistry and Sr-Nd isotopes for such a study. The apatite crystals are from four Cretaceous coeval granodiorite intrusions with different styles of hydrothermal mineralization in the Tongling ore district, South China. The selected intrusions are Hucun, Dongguashan, and Xinwuli, which host both porphyry and skarn Cu deposits, and the Chaoshan, which hosts a skarn Au deposit. The abundances of apatite major and trace elements, such as Mn, V, Ce, S, F, Cl, and Cu, together with the whole-rock compositions, are used to decipher the oxidation states, volatile compositions, and Cu fertility of the parental magmas. The apatite Sr-Nd isotope compositions are used as tracers for the magma sources. The results show that: (1) the parental magma of the Au-mineralized intrusion is less oxidized and has higher S-Cl contents than those of the Cu-mineralized intrusions, and (2) the proportion of mantle-derived melt is much higher in the former than in the latter. The results also reveal that the Cu-mineralized intrusions have highly variable apatite Cu-Cl-S compositions. Specifically, the Xinwuli intrusion has much higher Cu but lower Cl-S contents in apatite than the other two intrusions, indicating that a Cu-rich magma is not universally required for the formation of hydrothermal Cu deposits. This study demonstrates that apatite is a robust petrogenetic and metallogenic indicator for porphyry and skarn-type Cu-Au ore deposits.

Keywords: Apatite, magma oxidation state, Sr-Nd isotopes, LA-ICP-MS, Cu and Au mineralization; High-Grade Metamorphism, Crustal Melting and Granite Magmas

Introduction

Porphyry and skarn-type Cu and Au deposits are important resources of these metals in the world (Cooke et al. 2005; Meinert et al. 2005; Sillitoe 2010). In light of their similar geochemical characteristics as strongly chalcophile elements (Peach et al. 1990), Cu and Au association is common in the porphyry and skarn-mineralized systems (Meinert et al. 2005; Sillitoe 2010). But Cu and Au could also be mineralized separately in porphyry and skarn deposits, although the ore-related plutons could be closely related in time and space. For example, the Cenozoic porphyries located in the Jinshajiang-Red River metallogenic belt, eastern Tibet can host Cu deposits (i.e., Machangjing and Tongchang) and Au deposits (i.e., Yao'an and Beiya) (Hou et al. 2006; Bi et al. 2009). As a result, there is a debate about the fundamental controls on the different styles of mineralization associated with granite plutons, such as hydrothermal Cu vs. Au mineralization. A popular view is that highly oxidized magma is required for the formation of a porphyry and skarn Cu or Au ore deposit because, under relatively more oxidized conditions, Cu and Au can be more easily transported by magma to upper crustal levels and become highly concentrated in the ore-forming magmatic fluids (e.g., Ballard et al. 2002; Richards 2015; Richards and Şengör 2017). However, a recent study found that the parental magma of an ore-barren granitic pluton in the Ailaoshan region, southwest China is as oxidized as those of some porphyry Cu ore deposits in northern Chile (Xu et al. 2019). Moreover, although the consensus is that high-metal abundance in magmas is favorable to Cu and Au mineralization (Sun et al. 2015), some new data from melt inclusion studies do not show higher metal contents in the parental magmas for ore-bearing plutons than that for ore-barren plutons (Lerchbaumer and Audėtat et al. 2013; Zhang and Audétat 2017).

In the past, whole-rock geochemical data alone were used to determine the oxidation states and metal fertility of granitic pluton but only yielded limited success, mainly due to the fact that whole-rock compositions rarely preserve the original magma compositions, especially those that have experienced pervasive hydrothermal alteration and weathering. Apatite [$Ca_5(PO_4)_3F$] is a common accessory phase and an important sink for halogens and some trace elements in granites. Unlike some rock-forming minerals in these rocks, such as feldspars, biotite, and hornblende, apatite is much less susceptible to hydrothermal alteration and weathering (Ekstrom 1972; Ayers and Watson 1991; Creaser and Gray 1992). In addition, the fundamental controls

* E-mail: huruizhong@vip.gyig.ac.cn
† Special collection papers can be found online at http://www.minsocam.org/MSA/AmMin/special-collections.html.

0003-004X/21/0012–1873$05.00/DOI: https://doi.org/10.2138/am-2021-7497

on apatite crystallization and composition are well understood, owning to many excellent experimental studies (e.g., Watson 1979, 1980; Harrison and Watson 1984; Jahnke 1984; Pichavant et al. 1992; Wolf and London 1994, 1995; London et al. 1999). For example, we now know that apatite can crystallize early in some intermediate-felsic magmas based on experimental results (e.g., Harrison and Watson 1984) and the textural observations of natural samples such as the presence of apatite inclusions enclosed in feldspar, biotite, and hornblende in some granodiorites (e.g., Ding et al. 2015; Qian et al. 2019 and this study). The temperature interval of apatite crystallization from granitic magma is relatively small, mainly within 60–100 °C after magma begins to saturate with apatite (Piccoli and Candela 1994, 2002). The concentrations of REE, Sr, Cl, F, S, Eu, and Ce in apatite are a function of magma composition, temperature, and redox condition (Sha and Chappell 1999; Tepper and Kuehner 1999; Belousova et al. 2001, 2002; Piccoli and Candela 2002; Cao et al. 2012; Miles et al. 2014). For the reasons mentioned above, plus the recent advances in in situ analytical techniques for trace elements and isotopes, apatite is now widely used to study ore genesis associated with magma evolution (e.g., Sha and Chappell 1999; Imai 2002, 2004; Tollari et al. 2008; Huang et al. 2019; Sun et al. 2019; Mercer et al. 2020).

In this study, we use the trace elements (measured using LA-ICP-MS) and Sr-Nd isotopes (determined using LA-MC-ICP-MS) of apatite from four granodiorite intrusions in the Tongling ore district, plus complementary whole-rock data, to evaluate the magmatic controls on the different styles of hydrothermal mineralization, i.e., Cu vs. Au mineralization in the region. Our new data show significant compositional differences of apatite in the host rocks with the different styles of mineralization. The results from this study confirm that apatite is a robust petrogenetic and metallogenic indicator for porphyry and skarn-type ore systems.

Geological background

The Tongling region is an important ore district of the Middle-Lower Yangtze metallogenic belt that is situated in the northeastern part of the Yangtze block (Fig. 1a). In this region, Paleozoic-Mesozoic sedimentary rocks overlie Precambrian metamorphic rocks (Deng et al. 2011; Cao et al. 2017). Early-Middle Triassic carbonates are the country rocks of many younger granodiorite plutons with Cu, Au, Fe, and Mo mineralization in the Tongling ore district.

Spatially, the Middle-Lower Yangtze metallogenic belt is close to the continental collision zone between the North China block and the Yangtze block (Fig. 1a). The collision took place in the Middle Triassic, producing a series of NE-trending folds and major faults (Xie et al. 2012). From Late Jurassic to Early Cretaceous, the region underwent post-collisional extension, resulting in lithospheric delamination and associated voluminous magmatism (Xu et al. 2002; Wang et al. 2006). Meanwhile, the Paleo-Pacific plate was subducting beneath eastern China (Zhou et al. 2006; Li and Li 2007; Sun et al. 2007). Some granodiorite intrusions emplaced between 150 and 134 Ma in the Tongling region host hydrothermal Cu and Au ore deposits (Fig. 1b; Deng et al. 2011). Four of them were selected for this study. They are the Hucun, Dongguashan, and Xinwuli intrusions that host both

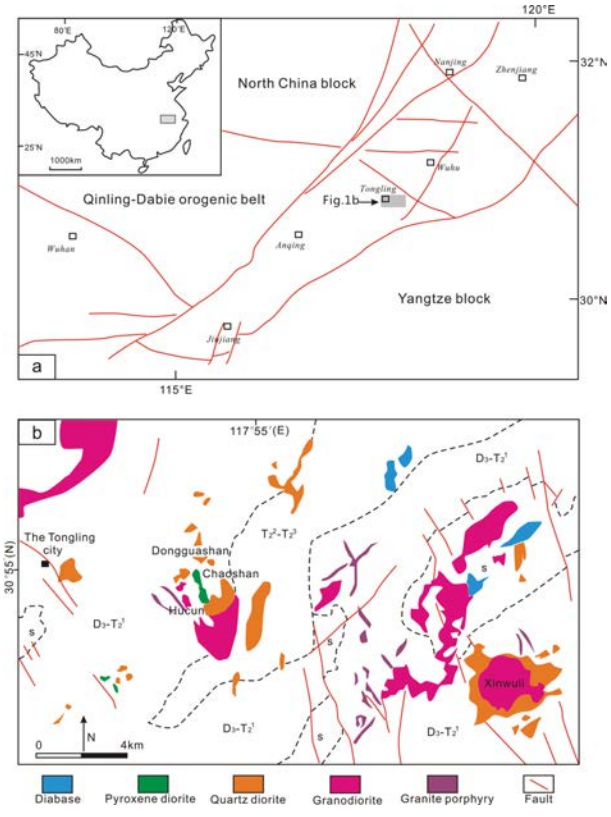

Figure 1. Regional geological map of the research area (modified from Liu et al. 2019).

porphyry- and skarn-type Cu ore deposits, and the Chaoshan intrusion that hosts only a skarn-type Au ore deposit (Lu et al. 2007; Yang et al. 2008; Cao et al. 2017; Wang et al. 2018; Liu et al. 2019).

The Au-mineralized intrusion

The Chaoshan intrusion is located ~7 km southeast of Tongling city. It intrudes Early-Middle Triassic limestones and shales. The exposure of this intrusion measures ~0.3 km^2 (Fig. 2a). It is mainly composed of pyroxene diorite that contains ~70% plagioclase, ~10% pyroxene, ~15% hornblende, and ~5% biotite. The accessory minerals include apatite and zircon. Apatite occurs mainly as euhedral crystals surrounded by biotites (Figs. 3a–3c). Skarns are common at the contacts with limestones. Some of the skarns contain Au mineralization, with an average Au grade of 18.4 g/t (Wang et al. 2008b). Gold mainly occurs as native Au inclusions enclosed in pyrrhotite, pyrite, and arsenopyrite crystals. Pyrrhotite separates from the Au-bearing samples yield a Re-Os isochron age of 141.7 ± 9.9 Ma (Wang et al. 2008a); indistinguishable with the SHRIMP zircon U-Pb age of the associated pyroxene diorite (142.9 ± 1.1 Ma) (Wang et al. 2004). The H-O isotope compositions of fluid inclusions are within the range of magmatic fluids (Yang et al. 2008). The isotope compositions of S, C, and O in the Au-bearing sulfides and gangue minerals such as calcite indicate that these elements are mainly derived from the parental magma of the pyroxene diorite (Wang et al. 2008b).

The Cu-mineralized intrusions

The Hucun intrusion was emplaced into the Carboniferous-Triassic sedimentary strata. It covers an area of 0.35 km^2 (Fig. 2a). This intrusion is dominated by medium- to coarse-grained granodiorite that is composed of ~40% plagioclase, ~25% quartz, ~15% K-feldspar, ~15% hornblende, and ~5% biotite. The accessory minerals are apatite, zircon, and titanite. Apatite mainly occurs as euhedral crystals surrounded by plagioclase and hornblende (Figs. 3d–3f). Skarns are present at the contacts with limestones in places. Some exoskarn zones contain Cu mineralization with grades from 0.4–0.8 wt% Cu (Cao et al. 2017). Porphyry-type Cu mineralization occurs at ~1000 m below the present surface within the intrusion. The ore minerals include chalcopyrite, pyrrhotite, pyrite, and minor molybdenite. SHRIMP zircon U-Pb age of the intrusion is 140.0 ± 2.6 Ma (Xu et al. 2008a). The fluid compositions and C-H-O isotopes indicate that the ore-forming fluids were mainly derived from the parental magma of the intrusion (Lu et al. 2007; Cao et al. 2017).

The Dongguashan intrusion is surrounded by the Upper Devonian to Lower Triassic sedimentary country rocks (Fig. 2a). This intrusion is composed of medium- to coarse-grained quartz diorite that is composed of ~60% plagioclase, ~15% quartz, ~15% hornblende, ~5% biotite, and ~5% K-feldspar. The accessory minerals include apatite, titanite, and zircon. Apatite mainly occurs as euhedral crystals surrounded by plagioclase (Figs. 3g–3i). The zircon U-Pb age of this intrusion is 140.3 ± 2.0 Ma (Wang et al. 2015). Both porphyry and skarn-type Cu mineralizations, which together contain 0.94 Mt Cu at 1 wt% Cu, occur within the intrusion and in the contacts with limestone in places (Wang et al. 2015). Stratiform orebodies are present in the sedimentary sequence up to 1000 m away from the contacts. Fluid inclusion data and H-O-S-Pb isotopes indicate that the ore-forming fluids were primarily derived from the parental magma of the intrusion (Xu et al. 2008b; Liu et al. 2019).

The Xinwuli intrusion is situated farther away from the Tongling City than the other selected intrusions described above (Fig. 1b). This intrusion covers an area of nearly 10 km^2. The country rocks are Triassic limestone and dolomitic limestone. The Xinwuli intrusion consists of quartz diorite in the margin and granodiorite in the center (Fig. 2b). This may be a result of multiple pulses from the same magma chamber at depth (Shao et al. 2007). Quartz diorite is medium- to fine-grained. It is composed of ~60% plagioclase, ~15% hornblende, ~10% quartz, ~10% biotite, and ~5% K-feldspar. Granodiorite is also medium- to fine-grained. It is composed of ~45% plagioclase, ~25% quartz, ~15% K-feldspar, ~10% hornblende, and ~5% biotite. The accessory minerals include apatite, titanite, and zircon. Apatite in this granodiorite intrusion occurs as euhedral crystals surrounded by plagioclase (Figs. 3j–3l). Both porphyry- and skarn-type Cu mineralizations are associated with this intrusion in several places. At Fenghuangshan, the skarn-type Cu mineralization is predominant, containing a total 0.40 Mt of Cu with an average ore grade of 1.24 wt% Cu (Pan and Dong 1999). The molybdenite Re-Os age is 141.7 ± 0.82 Ma and the zircon U-Pb age of the associated granodiorite is 143.1 ± 1.6 Ma (Li et al. 2014). The C-O-S isotopes of hydrothermal calcite and sulfides from the Fenghuangshan Cu deposit support the interpretation that the ore-forming fluids were mainly derived from the parental magma of the granodiorite intrusion (Wang et al. 2018).

Analytical methods

Whole-rock compositions

The whole-rock samples used in this study are relatively fresh and do not show significant Cu-Au mineralization. The concentrations of major elements in the selected rocks were determined with fused lithium tetraborate glass pellets using an Axios PW4400 X-ray fluorescence spectrometer at the State Key Labora-

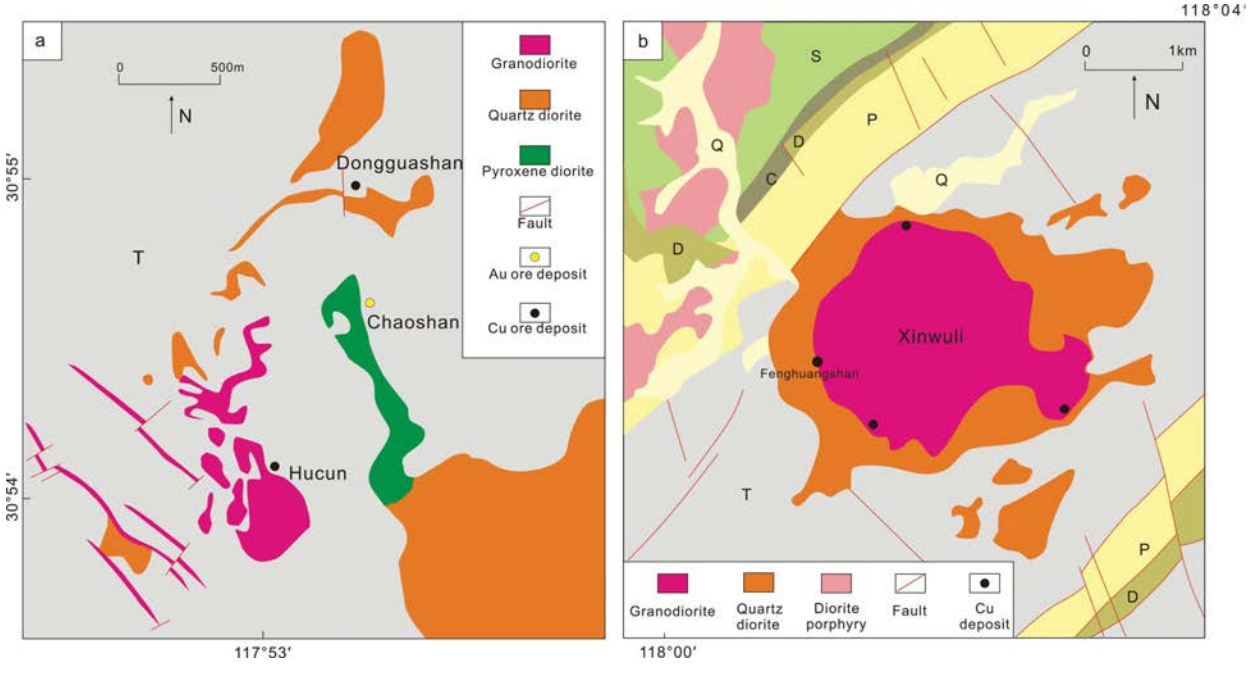

Figure 2. Simplified geological maps for the Chaoshan, Dongguashan, and Hucun intrusions (**a**) and the Xinwuli intrusion (**b**).

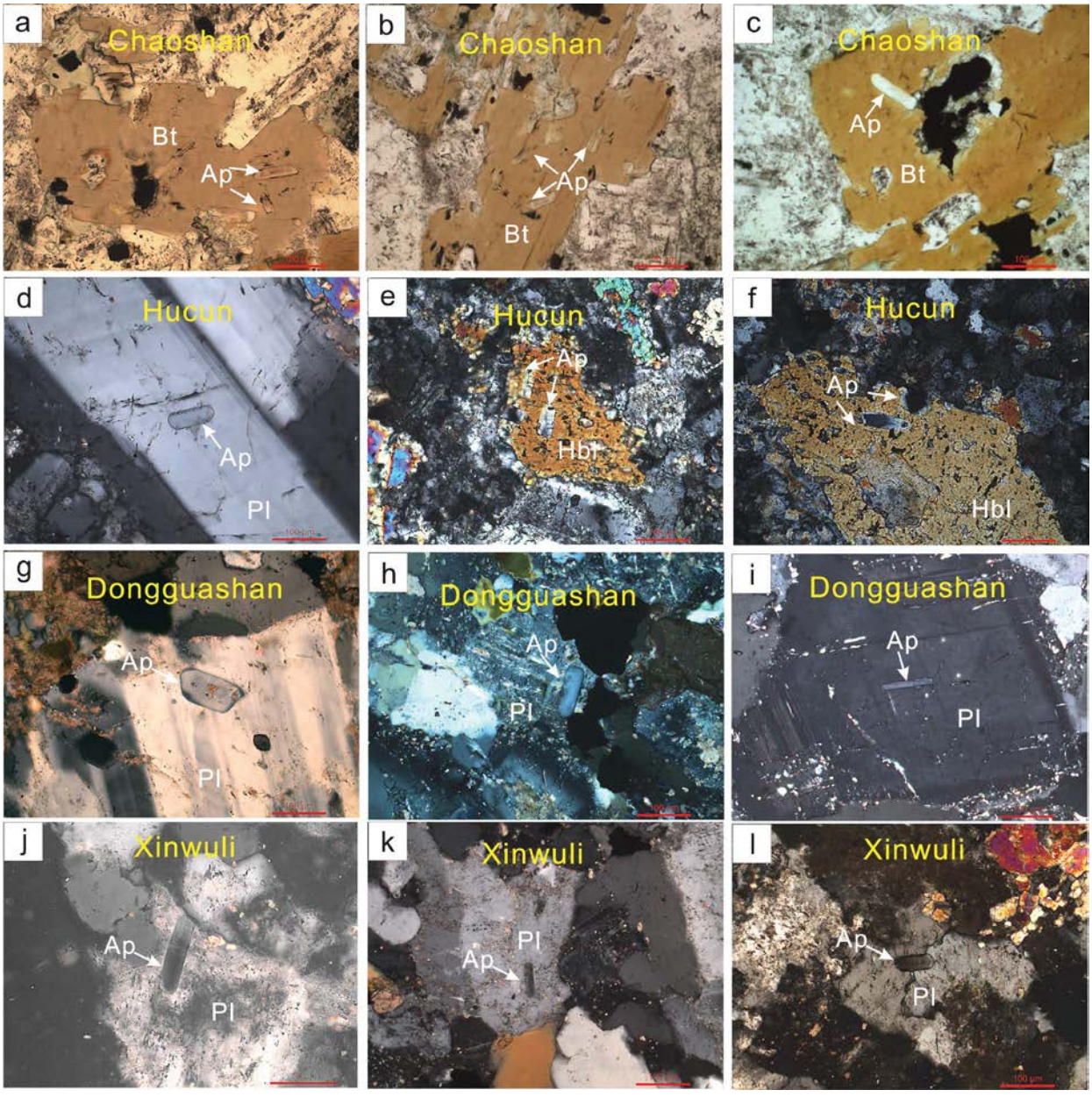

Figure 3. The modes of occurrence of apatite in the rock samples from the selected intrusions. Ap = apatite; Bt = biotite; Hbl = hornblende; Pl = plagioclase; Hbl = hornblende; Pl = plagioclase; Qtz = quartz; Ttn = titanite.

tory of Ore Deposit Geochemistry, Institute of Geochemistry, Chinese Academy of Sciences in Guiyang (SKLODG). The analytical uncertainty is estimated to be <5%. The concentrations of trace elements in the whole rocks were analyzed using a PE DRC-e ICP-MS at the SKLODG. Powdered samples (50 mg) were dissolved using mixtures of HF and HNO_3 in high-pressure polytetrafluoroethylene vessels for 2 days at ~190 °C. Rh was used to monitor signal drift during the analysis. The detailed analytical procedures are described in Qi et al. (2000). The analytical uncertainty is estimated to be within 10%.

Apatite major elements compositions

Apatite crystals were separated from the samples using standard heavy-liquid and magnetic methods and then mounted and polished in epoxy. Targets suitable for the in situ analysis were chosen using CL and BSE images. The contents of major and minor elements in apatite (n = 123) were determined using a EPMA-1600 electron microprobe at the SKLODG. The analytical conditions were: 25 kV accelerating voltage, 10 nA beam current, and 10 μm beam diameter. The electron beam was oriented perpendicular to the apatite c-axis to minimize the error for F analysis (Stormer et al. 1993; Goldoff et al. 2012). The following natural minerals were used for calibration: kaersutite (Ca, Mn, Na, Al, Si, Fe), tugtupite (Cl), and apatite (P, S, F).

Apatite and zircon trace elements compositions

The concentrations of trace elements in apatite (n = 123) and zircon (n = 73) were measured by in situ LA-ICP-MS at the SKLODG. The LA-ICP-MS system was an Agilent 7500a ICP-MS equipped with a Resonetics RESOLution M-50 ArF-Excimer laser gun (λ = 193 nm, 80 mJ, 10 Hz). The laser ablation spot was 44 μm in diameter. The ablated aerosol was fed to the ICP instrument using He gas. The NIST610 and NIST612 standards were used for calibration. For apatite

analysis, the content of Ca was measured using ^{43}Ca and normalized using the concentration determined by electron probe analysis. Off-line data reduction was performed using ICPMSDataCal software from Liu et al. (2008). The detection limits of apatite by LA-ICP-MS are estimated to be <0.3 ppm for Sm and Gd, and <0.1 ppm for U, Th, Sr, Zr, Ga, Cu, and other REE. The detection limits of zircon by LA-ICP-MS are estimated to be <0.3 ppm for Sm and Gd, and <0.1 ppm for U, Th, Sr, Zr, Ga, and other REE.

Apatite Sr-Nd isotopes

In situ apatite Sr isotope measurements were conducted using a Nu Plasma III MC-ICP-MS (Nu Instruments) instrument equipped with a RESOlution-155 ArF193-nm laser ablation sampling system (Australian Scientific Instruments) at the SKLODG. Apatite was ablated in a mixture of helium (350 mL/min) and nitrogen (2 mL/min) atmosphere using the following parameters: 30 s baseline time, 40 s ablation time, 60–104 μm spot size, 6 Hz repetition rate, and 6 J/cm^2 energy density. The analytical procedure and interference correction are the same as those described in Ramos et al. (2004) and Gao and Zhou (2013). One in-house standard of a modern-day coral was measured after every five samples, and two apatite standards (AP1 and MAD) were analyzed after every thirty samples. The results were used for quality control. The measured $^{87}Sr/^{86}Sr$ ratio for the apatite standard AP1 was 0.71133 ± 0.00004 (n = 12), which was identical to the recommended value (AP1: 0.71136 ± 0.00008; Yang et al. 2014).

In situ apatite Nd isotope measurements were conducted in the same manner as the Sr isotope analysis. The interference of ^{144}Sm on ^{144}Nd was derived from the ^{147}Sm intensity with a natural $^{144}Sm/^{147}Sm$ ratio of 0.205484 (Isnard et al. 2005). The mass bias factor of Sm was calculated from the measured isotopic ratio of $^{147}Sm/^{149}Sm$ and its actual value 1.08680 (Isnard et al. 2005). The mass bias of $^{143}Nd/^{144}Nd$ was normalized to $^{146}Nd/^{144}Nd = 0.7129$ with an exponential law. One apatite standard (Durango) was analyzed after every five samples, and the other two apatite standards (AP1 and MAD) were analyzed after every 30 samples. The results were used for quality control. The measured $^{143}Nd/^{144}Nd$ ratio for the apatite standard AP1 was 0.512342 ± 0.000014 (n = 12), which was identical to the recommended value (AP1: 0.512352 ± 0.000024) (Yang et al. 2014).

Results

Whole-rock compositions

Whole-rock compositions are provided as Online Materials[1] OM1. These data indicate that the Hucun, Dongguashan, and Xinwuli intrusions have metaluminous and calc-alkaline compositions (Figs. 4a and 4b), with a Rittmann index [$\sigma = (Na_2O + K_2O)^2/(SiO_2 - 43)$, units in wt% (Rittmann 1957, 1962)] of 2.37–2.88 and an aluminum saturation index [ASI = molar ratio $Al_2O_3/(CaO+Na_2O+K_2O)$ (Zen 1986; Acosta-Vigil et al. 2003)] of 0.74–0.90. The Chaoshan intrusion has a metaluminous and alkaline composition (Figs. 4a and 4b), with a Rittmann index of 4.54–4.82 and an aluminum saturation index of 0.66–0.68. The intrusive rocks are all characterized by moderate to severe K-Nb,-P-Ti depletions (Fig. 4c) and significant light REE enrichments (Fig. 4d). The Dongguashan, Xinwuli, and Hucun intrusions show typical adakite trace element compositions, such as Sr > 400 ppm, Y < 20 ppm, Yb < 2 ppm, $(La/Yb)_N > 15$, and δEu > 0.80 (Defant and Drummond 1990). In contrast, the Chaoshan intrusion does not show such adakite characteristics.

Apatite major and trace elements

The ideal formula of apatite is simplified as $A_5(XO_4)_3Z$. The A-site usually accommodates Ca^{2+} and other minor or trace cations such as Sr^{2+}, Mn^{2+}, Fe^{2+}, $REE^{3+,2+}$, Y^{3+}, Ga^{2+}, and Na^+. The X site is mainly occupied by P^{5+} but can be substituted by other highly charged cations such as V^{5+}, S^{6+}, and C^{4+}. The Z site is occupied by F^-, Cl^-, and OH^-. Based on the F^-, Cl^-, and

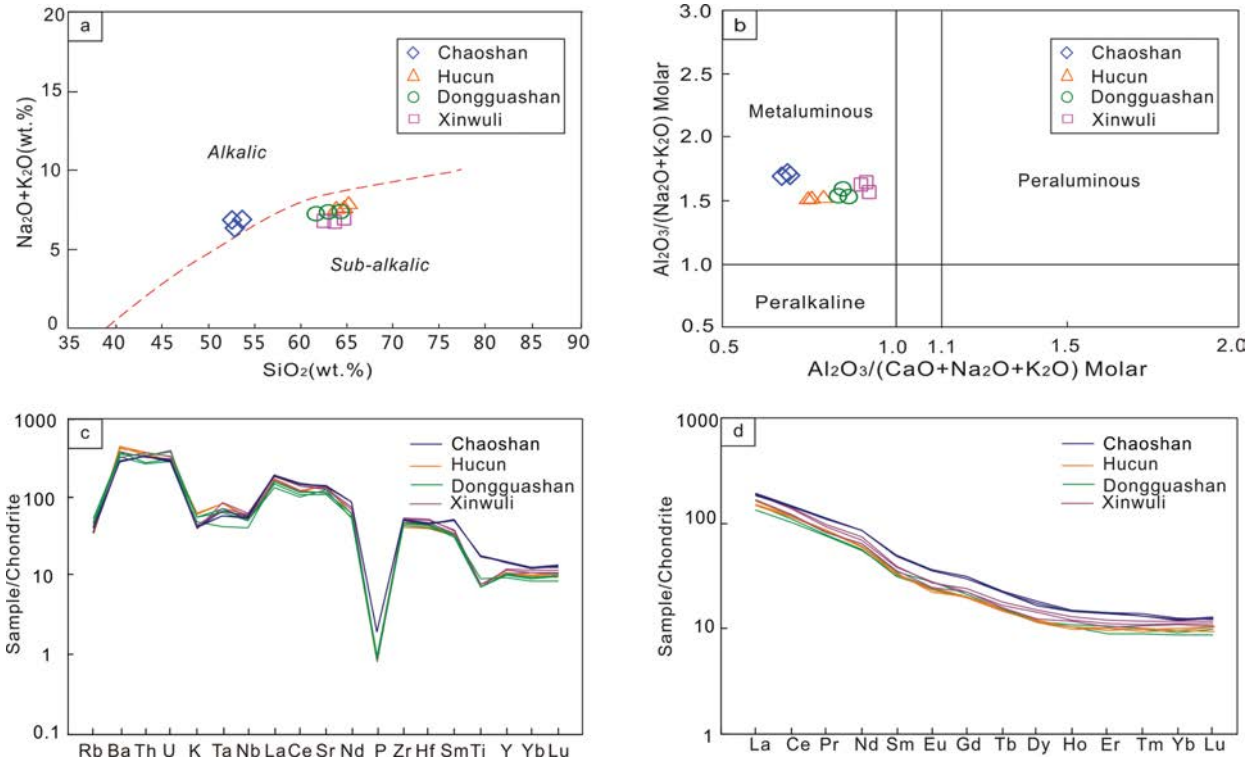

Figure 4. (Na_2O+K_2O) vs. SiO_2 diagram (Irvine and Baragar 1971) (**a**); A/NK vs. A/CNK diagram (Maniar and Piccoli 1989) for the Chaoshan, Hucun, Dongguashan, and Xinwuli intrusions (**b**); chondrite-normalized trace-element diagrams (**c**); and REE diagrams (**d**) for the selected intrusions. Data are listed in Online Materials[1] OM1. The chondrite values are from Sun and McDonough (1989).

OH^- compositions, apatite can be subdivided into fluorapatite, chloraptite, and hydroxylapatite. The contents of the major and trace elements in apatite are given as Online Materials[1] OM2.

Major elements (Ca-Mn-Na) in the apatite structure. The apatite crystals from the four selected intrusions have similar average CaO contents (54–55 wt%). The apatite average MnO contents are higher in the Hucun and Chaoshan intrusions (~0.10 wt%) and are lower in the Xinwuli (0.08 wt%) and Dongguashan intrusions (0.04 wt%). The negative correlation between apatite CaO and MnO indicates the equivalent substitution of Ca^{2+} by Mn^{2+} (Fig. 5a) (Pan and Fleet 2002). The apatite average Na_2O content is the lowest in the Xinwuli intrusion (mostly below the detection limit of EPMA), the highest in the Chaoshan intrusion (0.14 wt%), and intermediate in the Dongguashan (0.09 wt%) and Hucun (0.07 wt%) intrusions. The negative correlation of apatite Na_2O and CaO (Fig. 5b) is related to the following reactions (Rønsbo 1989; Sha and Chappell 1999):

$$Na^+ + S^{6+} = Ca^{2+} + P^{5+} \quad (1)$$
$$2Na^+ = Ca^{2+} \quad (2)$$
$$REE^{3+} + Na^+ = 2Ca^{2+}. \quad (3)$$

The positive correlation of apatite Na_2O and SO_3 in the Chaoshan intrusions (Fig. 5c) implies that reaction 1 could be dominant for these apatite crystals. However, the low-apatite SO_3 content and the negative correlation of apatite REE and CaO (Fig. 5d) suggest that reaction 3 is more prevalent in the Hucun, Dongguashan, and Xinwuli intrusions.

Major elements (P-S-F-Cl) in the apatite structure. The apatite crystals from the selected four intrusions have similar average P_2O_5 contents (40–41 wt%). The apatite average SO_3 contents are the highest in the Chaoshan intrusion (0.28 wt%), medium in the Hucun and Dongguashan intrusions (0.17 and 0.20 wt%, respectively), and the lowest in the Xinwuli intrusion (<0.16 wt%). S enters apatite by complex substitutions of:

$$S^{6+} + Si^{4+} = 2P^{5+} \quad (4)$$

and reaction 1 (Sha and Chappell 1999). The positive correlation of apatite CaO and P_2O_5 (Fig. 5e) responds well to reaction 1, while reaction 4 could be negligible because no Si was detected by EPMA in apatite. The observed negative correlation of apatite F and Cl (Fig. 5f) supports the reciprocal substitution of these two elements (Pan and Fleet 2002). Our data show that the Chaoshan intrusion has a relatively high-apatite Cl content (average of 0.45 wt%) and a relatively low-apatite F content (average of 2.44 wt%) and F/Cl ratio (average of 6.2). The apatite crystals from the Xinwuli, Hucun, and Dongguashan intrusions have relatively low-Cl contents (averages of 0.11, 0.32, and 0.33 wt%, respectively) and relatively high-F contents (averages of 2.89, 2.76, and 2.52 wt%, correspondingly) and F/Cl ratios (averages of 29.5, 10.6, and 8.2, respectively).

Minor elements (REE-Y) in the apatite structure. Among the four selected rocks, the apatite total REE content is the highest in the Chaoshan intrusion (average of 7035 ppm), intermediate in the Xinwuli intrusion (average of 6410 ppm), and the Dongguashan intrusion (average of 5469 ppm), and the lowest in the Hucun intrusion (average of 4771 ppm). The magnitude of the REE content in apatite is consistent with that in whole-rock samples. The negative correlation of apatite CaO and REE (Fig. 5d) has implications for the substitution of Ca by REE through reactions that include:

$$2REE^{3+} + \square = 3Ca^{2+} \quad (5)$$

and reaction 3 (Pan and Fleet 2002; Rønsbo 1989; Sha and Chappell 1999). Reaction 3 could be important in the Hucun and Chaoshan intrusions because of the positive correlation of REE and Na_2O (Fig. 5g). The chondrite- normalized REE patterns of apatite from the four selected intrusions (Fig. 6) show light REE enrichments relative to heavy REE and a significantly negative Eu anomaly (0.3–0.6). Apatite crystals from the Chaoshan and Xinwuli intrusions have higher Y contents (averages of 482 and 413 ppm, respectively) than those from the Hucun and Dongguashan intrusions (averages of 236 and 268 ppm, respectively). The observed positive correlation of apatite Y and REE (Fig. 5h) hints at the similar partitioning behavior of these two elements as the substitute of Ca in apatite.

Trace elements (Sr-Th-U) in the apatite structure. Apatite is a relatively Sr-, Th-, and U-rich mineral (Belousova et al. 2002; Chu et al. 2009). The apatite average Sr contents are identical in the Chaoshan, Hucun, and Xinwuli intrusions (averages of 720, 751, and 714 ppm, respectively) but are much lower in the Dongguashan intrusion (343 ppm). The apatite from the Xinwuli intrusion has higher Th and U contents (averages of 116 and 34 ppm, respectively). Lower contents of Th (averages of 30, 22, and 20 ppm) and U (averages of 8.9, 7.0, and 5.9 ppm) are observed in apatite from the Chaoshan, Dongguashan, and Hucun intrusions, respectively.

Trace elements (Ga-V-Cu-Cr) in the apatite structure. These four elements in apatite are considered to be potential monitors of magma composition and oxidation state (Sha and Chappell 1999; Mao et al. 2016; Sun et al. 2019). Thus, we determined the concentration variations of these elements in our apatite samples. The data show that apatite from the Chaoshan intrusion contains more Ga (average of 20 ppm) than that from the other three intrusions (14–17 ppm). The apatite average V content is higher in the Chaoshan and Xinwuli intrusions (~17 ppm) than that in the Hucun (8.7 ppm) and Dongguashan (11 ppm) intrusions. The apatite Cu content is an order of magnitude lower in the Hucun, Dongguashan, and Chaoshan intrusions (<0.5 ppm) than that in the Xinwuli intrusion (average of 4.2 ppm). The apatite crystals from these four intrusions have similar average Cr content, ranging from 1.5 to 1.6 ppm.

Apatite Sr-Nd isotopes

The in situ Sr-Nd isotopic data of apatite are provided as Online Materials[1] OM3. Apatite from the Chaoshan intrusion has $^{87}Sr/^{86}Sr$ ratios from 0.70638 to 0.70683 and εNd(0) values from −11.6 to −8.3. Overall, apatite from the Hucun intrusion has slightly higher $(^{87}Sr/^{86}Sr)_i$ ratios (0.70718 to 0.70812) and lower εNd(0) values (−15.1 to −8.6). Apatite from the Xinwuli and Dongguashan intrusions has the highest $(^{87}Sr/^{86}Sr)$ ratios (0.70820 to 0.70895 and 0.70802 to 0.71091, respectively) and the lowest εNd(0) values (−16.3 to −10.8 and −16.6 to −12.1, respectively) among the four studied intrusions. The current and initial $^{87}Sr/^{86}Sr$ ratios of apatite are likely very similar because

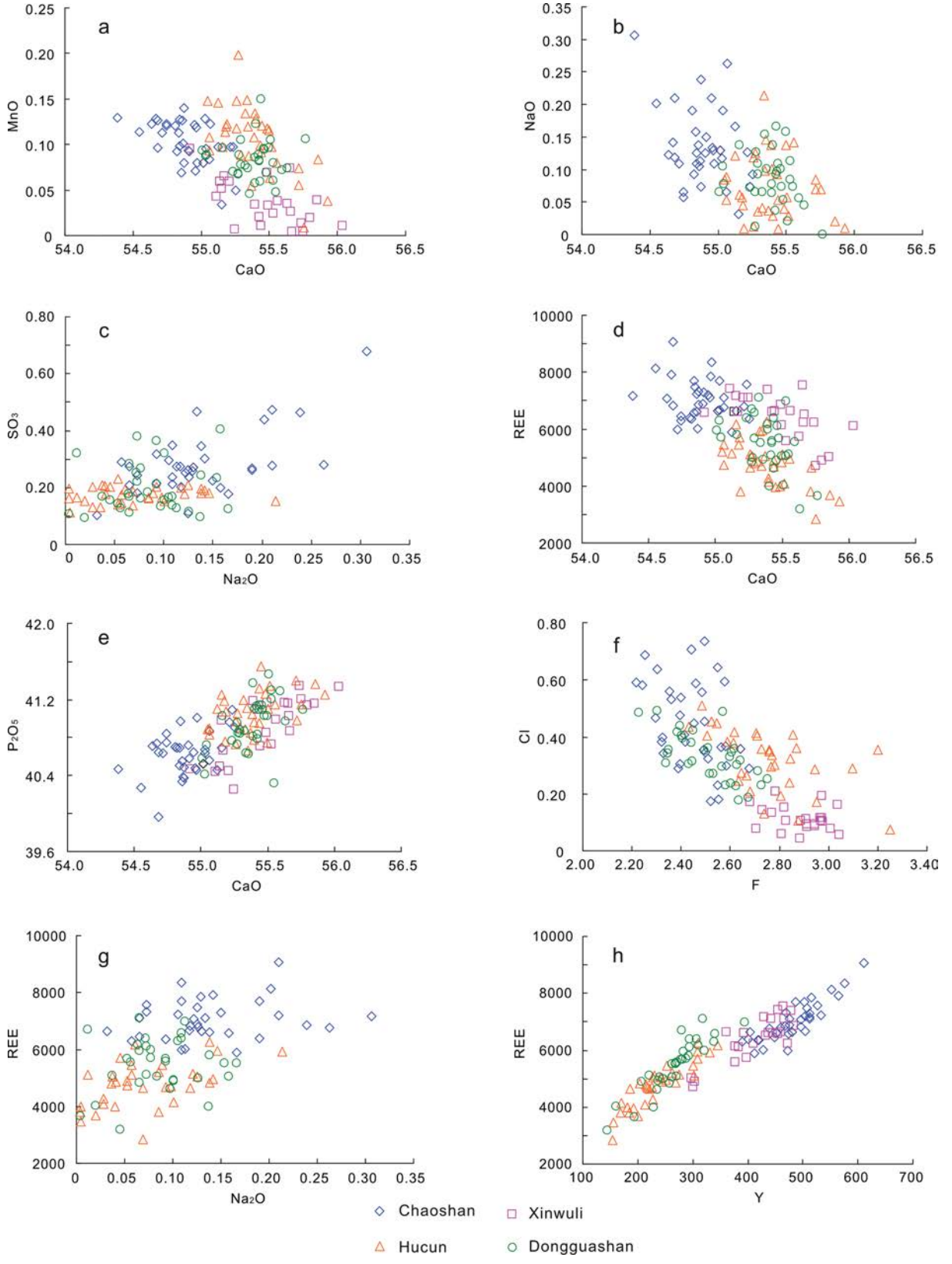

Figure 5. Plots of CaO vs. MnO (**a**); CaO vs. Na_2O (**b**); Na_2O vs. SO_3 (**c**); CaO vs. REE (**d**); CaO vs. P_2O_5 (**e**); F vs.Cl (**f**); Na_2O vs. REE (**g**); and Y vs. REE (**h**) in apatite from the selected intrusions.

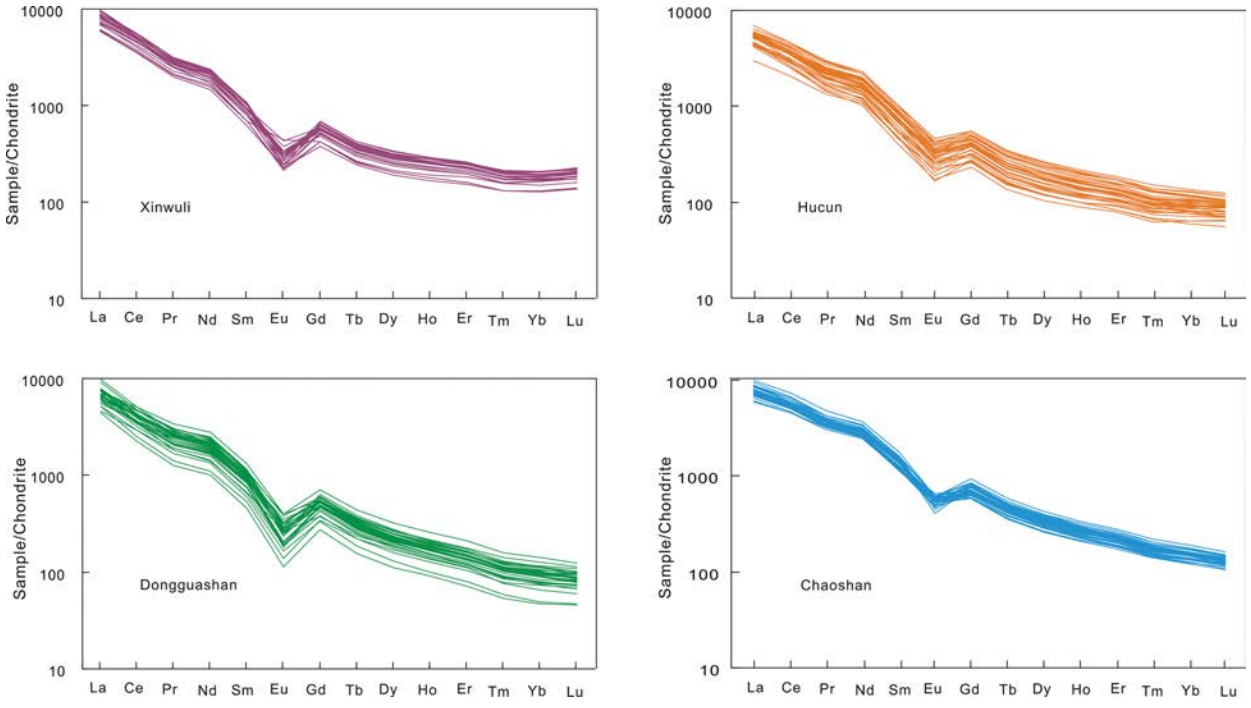

Figure 6. Chondrite-normalized REE patterns for apatite from the selected intrusions. Data are listed in Online Materials[1] OM2. The chondrite values are from Sun and McDonough (1989).

Rb content in the apatite structure is negligible (Sun et al. 2019). The calculated initial εNd(t) values of apatite based on the previously reported ages for the intrusions are as follows: from −9.9 to −6.6 for Chaoshan, from −13.1 to −6.6 for Hucun, from −14.3 to −8.9 for Xinwuli, and from −14.8 to −10.0 for Dongguashan.

Trace elements in zircon

The average contents of some trace elements in zircon are given as Online Materials[1] OM4. High-Th/U ratios (>0.1) confirm that the zircon crystals used in this study are all magmatic. The zircon average Ce contents are 76, 20, 31, and 30 ppm in the Chaoshan, Xinwuli, Dongguashan, and Hucun intrusions, respectively. The zircon average Ti contents are 20, 6.3, 5.9, and 3.6 ppm in the Chaoshan, Xinwuli, Dongguashan, and Hucun intrusions, respectively. We calculated the zircon Ce^{4+}/Ce^{3+} ratio using the method proposed by Ballard et al. (2002). The calculated Ce^{4+}/Ce^{3+} ratios of zircon are included in the Online Materials[1] OM4, which show that zircon from the Chaoshan intrusion has a lower zircon Ce^{4+}/Ce^{3+} ratio (average of 31) than that from the Dongguashan, Xinwuli, and Hucun intrusions (average ratios 135, 155, and 274, respectively). We estimated the temperature of early magmas using Ti-in-zircon thermo-metry proposed by Ferry and Watson (2007). The calculated temperatures of magmas are 957, 815, 757, and 807 °C in the Chaoshan, Xinwuli, Hucun, and Dongguashan intrusions, respectively (Table 1).

Discussion

Apatite origin

The apatite crystals from all four intrusions are interpreted to be of magmatic origin, not hydrothermal or metamorphic origin. The reasons are as follows. First, the chemical compositions, such as the ranges of Mn, Ca, Na, F, Cl, and H_2O contents

Table 1. Estimation of magmatic oxygen fugacity and the contents of S, Cl, and F using apatite compositions

Intrusion	Average apatite Mn (ppm)	Average apatite SO_3 (ppm)	Average apatite F (wt%)	Average apatite Cl (wt%)	Average magmatic SO_3 content (ppm)[a]	Average magmatic SO_3 content (ppm)[b]	Average magmatic F content (ppm)[c]	Average magmatic Cl content (ppm)[c]	Zircon Ti temperature (°C)[d]	ΔFMQ[e]
Chaoshan	797	2834	2.44	0.45	116	1067	814	5568	957	+0.1
Xinwuli	279	560	2.89	0.11	27	23	963	1415	815	+3.8
Hucun	813	1747	2.76	0.32	58	24	919	3994	757	+3.9
Dongguashan	646	1977	2.52	0.33	67	69	839	4130	807	+3.2

[a] Calculated equation of magmatic SO_3 content is from Peng et al. (1997): $\ln K_D (SO_3)_{apatite}/(SO_3)_{melt} = 21130/T - 16.2$.
[b] Calculated equation of magmatic SO_3 content is from Parat et al. (2011): SO_3 apatite (wt%) = 0.157 × ln SO_3 glass (melt, wt%) + 0.9834.
[c] Partition coefficients of F and Cl are from Parat et al. (2011). Dcl apatite/melt = 0.8; DF apatite/melt = 30.
[d] Ti-in-zircon thermo-metry is from Ferry and Watson (2007): log (Ti in zircon ppm) = 5.711 ± 0.072–(4800 ± 86)/T(K) – log a_{SiO_2} + log a_{TiO_2}. a_{SiO_2} is equal to1.0 and a_{TiO_2} is equal to 0.5. Apatite saturation temperature cannot represent the temperature of massive crystallization of apatite in the intermediate magma (Piccoli and Candela 2002). Instead, Ti-in-zircon thermometry could better reveal the temperature of early magma because this calculation can avoid the error caused by the use of whole-rock compositions as parameters to represent magmatic compositions.
[e] Fayalite-magnetite-quartz (FMQ) oxygen fugacity buffer is from Myers and Eugster (1983). The calculated equation of oxygen fugacity using apatite Mn is from Miles et al. (2014): log (f_{O_2}) = –0.0022 (±0.0003) Mn(ppm) – 9.75(±0.46).

in the analyzed apatites, are generally consistent with those of magmatic origin that occur elsewhere in the world (Piccoli and Candela 2002) (see Fig. 7). Second, hydrothermal apatite commonly has very high Cl, exceeding 3.0 wt%, coupled by low-F content (Palma et al. 2019), which is likely due to a much higher abundance of Cl than F in the parental hydrothermal fluids (Candela 1986; Warner et al. 1998). The high-*T* hydrothermal alteration (e.g., K silicate alteration) may alter apatite composition (Bouzari et al. 2016), resulting in Cl enrichment in the apatite (Palma et al. 2019). However, the apatite crystals from the selected intrusions all have low-Cl contents (<0.75 wt%). Third, the apatite crystals used in this study all have higher Th (>10 ppm) and La (>1000 ppm) contents than typical metamorphic apatite (Th < 10 ppm and La < 1000 ppm; Henrichs et al. 2018). Finally, the interpretation of a magmatic origin for the apatite crystals used in this study is supported by the textural relationships, such as their occurrence as inclusions of euhedral grains enclosed in plagioclase, biotite, and hornblende (Fig. 3), indicating that the apatite crystals could crystallize before the crystallization of the host silicate minerals. Using the method of Harrison and Watson (1984) and whole-rock compositions, the calculated apatite saturation temperatures in the studied intrusive rock are >890 °C (Online Materials[1] OM1), further supporting a magmatic origin for the apatite crystals in these rocks.

Magmatic oxidation state

The traditional method that uses the whole-rock Fe^{3+}/Fe^{2+} ratio to determine a magmatic oxidation state may be inaccurate owing to the effect of alteration and weathering on the ratio. The compositions of alteration-resistant minerals such as apatite may be more accurate magmatic redox proxies. Many researchers have demonstrated that the variations of Eu, Ce, Mn, V, and Ga in apatite are related to the changes of magmatic oxidation states (e.g., Drake 1975; Sha and Chappell 1999; Streck and Dilles 1998; Imai 2002, 2004; Boechat et al. 2003; Cao et al. 2012; Sun et al. 2019). Eu^{3+}, Ce^{3+}, Mn^{2+}, V^{5+}, and Ga^{2+} are favored by apatite because Eu^{3+}, Ce^{3+}, Mn^{2+}, and Ga^{2+} can occupy the heptahedral Ca site while V^{5+} can occupy the tetrahedral P site (Piccoli and Candela 2002). A higher oxygen fugacity increases Eu^{3+}, Ce^{4+}, Ga^{3+}, Mn^{3+}, and V^{5+} at the expense of Eu^{2+}, Ce^{3+}, Ga^{2+}, Mn^{2+}, and V^{4+} in magma, which facilitates the incorporation of Eu and V, rather than Ce, Mn, and Ga into apatite. As a result, the apatite crystallizing from more oxidized magma will contain more Eu and V but less Ga, Mn, and Ce than that crystallizing from less oxidized magma if the concentrations of these elements are constant in the various magmas. However, the use of these proxies to trace magmatic oxidation states requires careful consideration of elemental partitioning behaviors in different mineral phases coexisting with apatite. For example, feldspar crystallization can remove large amounts of Eu and Sr from the coexisting melt (Ballard et al. 2002; Bi et al. 2002; Buick et al. 2007). The positive correlation of apatite δEu and Sr (Fig. 8a) means that apatite δEu value and Sr content are profoundly affected by feldspar crystallization in the selected intrusions. Similarly, Ga is compatible with feldspar because it can substitute for Al (Bedard 2006). The simultaneous decrease of Ga and Sr contents in apatite from the Hucun and Dongguashan intrusions (Fig. 8b) indicates that the low-Ga content in the apatite crystals may have resulted from feldspar crystallization. Based on this finding, the δEu and Ga content in apatite is not a suitable index to delineate the magmatic oxidation state in the intrusions from this study.

Despite the limitations, some apatite proxies are still useful, including V concentration. Our data reveal that the Chaoshan intrusion has much higher whole-rock V content (>200 ppm) than the Xinwuli intrusion (<100 ppm), but apatite from the former intrusion does not have higher V contents. Early crystallization of clinopyroxene from the parental magma for the Chaoshan intrusion may explain lower V content than expected in the apatite crystals from this intrusion. Cr is highly compatible in the clinopyroxene structure (e.g., Johnston and Schwab 2004). Thus, this element may be used to track the effect of clinopyroxene crystallization on the compositions of magma and the apatite crystallizing from the fractionated magma. If a decrease of V content in apatite is due to early clinopyroxene crystallization, a decrease of Cr content in apatite should also occur. Nevertheless, no simultaneous reduction of these elemental contents is observed in the apatite crystals from the Chaoshan intrusion (Fig. 8c). Experimental results showed that V, unlike Cr, may behave as an incompatible element in the clinopyroxene structure when the oxidation state of the magmatic system is above the FMQ buffer (Mallmann and O'Neill 2009). This scenario is likely to prevail in the Chaoshan magmatic system, where the estimated magmatic oxygen fugacity is close to FMQ+0.1 (see below). Magnetite is rare in the Chaoshan intrusion. A previous study has shown that the onset of magnetite saturation usually occurs in magma where SiO_2 content reaches 60 wt% (Jenner et al. 2010). However, the whole-rock SiO_2 content of the Chaoshan intrusion is <55 wt%. This implies that the magnetite in this intrusion can only crystallize in the late stage of magma evolution, and thus the chemical composition of apatite that is an early mineral phase may not be affected by magnetite crystallization. Finally, the low-V content in hornblende (253–348 ppm) and clinopyroxene (151–237 ppm) from the Chaoshan intrusion

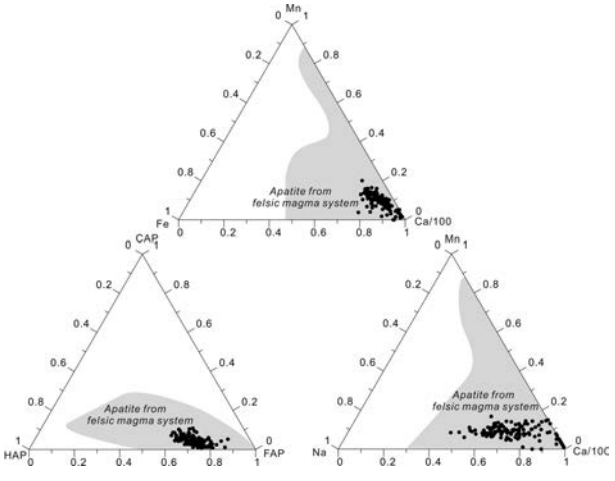

Figure 7. The molar ratio of Ca/100-Mn-Fe, Ca/100-Mn-Na, and fluorapatite (FAP)-chlorapatite (CAP)-hydroxylapatite (HAP) in apatite from the selected intrusions. The base map is from Piccoli and Candela (2002). The calculated method on the mole fraction of FAP, CAP, and HAP is from Piccoli and Candela (2002).

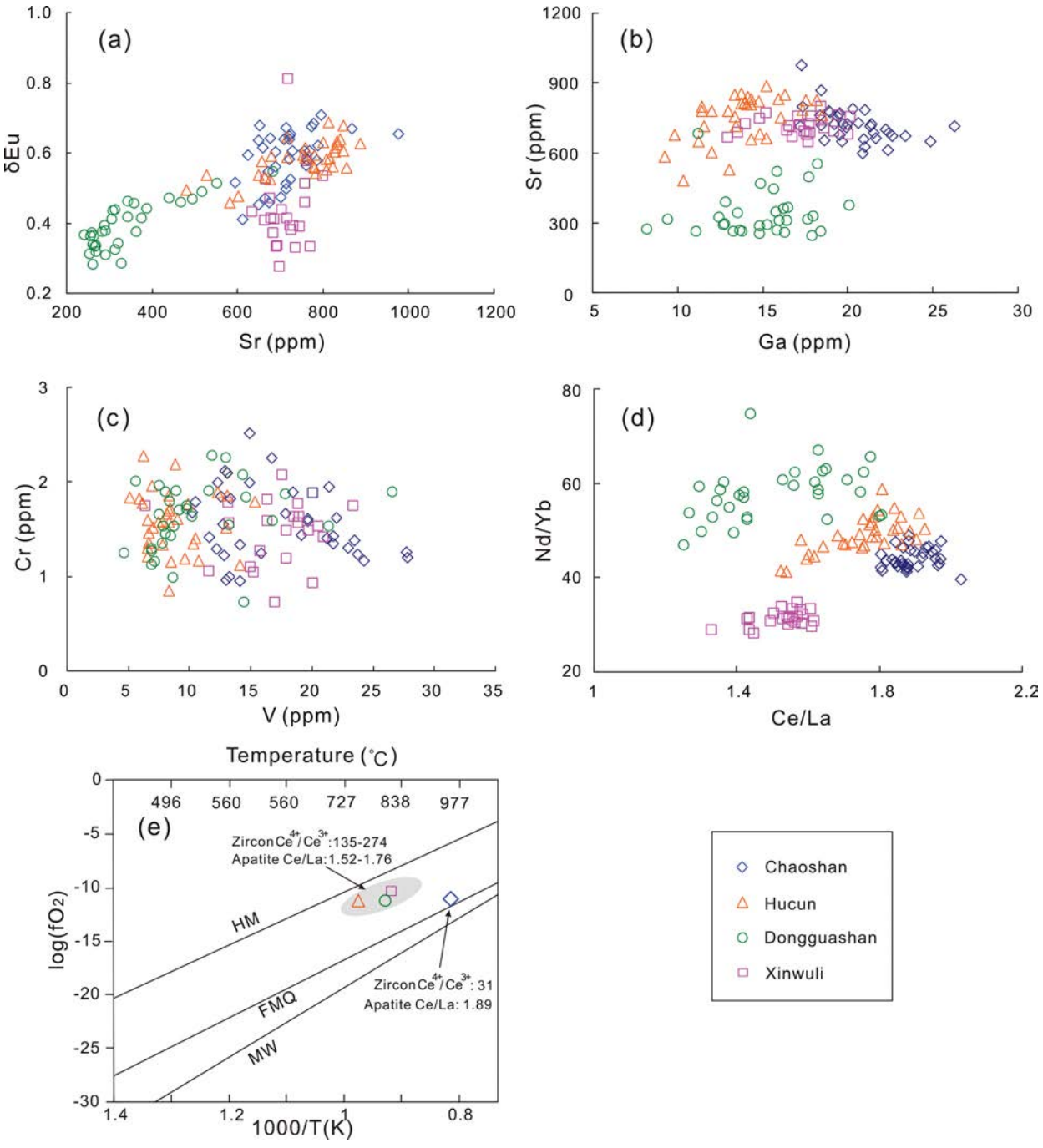

Figure 8. Plots of Sr vs. δEu (**a**); Ga vs. Sr (**b**); V vs. Cr (**c**); and Ce/La vs. Nd/Yb (**d**) in apatite from the selected intrusions and the estimated magma oxygen fugacity from Table 1 (**c**).

(Tu 2014) suggests that the amount of V removed from the melt via the crystallization of these minerals is limited. In view of the above findings, we infer that the crystallization of other minerals may fail to trigger a significantly downward V content in apatite from the Chaoshan intrusion. The lower V content than expected in apatite from the Chaoshan intrusion is mainly due to the relatively low-magmatic oxygen fugacity, which suppresses the incorporation of V into apatite.

The above inferred oxidation states can be further evaluated using the Ce/La ratios of apatite. Ce and La share chemical similarities and are difficult to fractionate during magma evolution unless some minerals that have greatly discrepant partition coefficients of La and Ce, such as zircon, are also crystallizing. Numerous experiments revealed that Ce is much more compatible than La in the zircon structure (Nardi et al. 2013; Rubatto and Hermann 2007). As a result, zircon crystallization may lead

to a decrease of Ce/La ratio in the apatite crystallizing from the fractionated magma. Similarly, zircon crystallization may increase the Nd/Yb ratio in the apatite because Yb is more compatible than Nd in zircon structure (Nardi et al. 2013). However, there is no negative correlation between Ce/La and Nd/Yb in the apatite crystals from the selected four intrusions (Fig. 8d). Since the Ce and La contents of zircon are nearly two orders of magnitude lower than that of coexisting apatite in the samples, it seems that zircon crystallization does not influence the Ce/La ratio of coexisting apatite. The whole-rock Ce/La ratio is uniform in the selected four intrusions (1.88–2.00), but the apatite from the Chaoshan intrusion has a higher Ce/La ratio (average of 1.89) than that from the other three intrusions (average of 1.52–1.76). This is probably due to the lower oxygen fugacity of the parental magma for the Chaoshan intrusion compared to that of other three intrusions. It follows that the relatively reduced conditions cause the increase of Ce^{3+} at the expense of Ce^{4+} in the melt and facilitate the incorporation of more Ce into apatite in the form of Ce^{3+} to substitute Ca. However, the content of La in apatite is independent of magmatic oxidation state because La^{3+} is the only major ionic form of this element. As a result, the change of oxygen fugacity cannot change the efficiency of La replacing Ca in apatite. In view of the above understanding, the higher Ce/La ratio in apatite from the Chaoshan intrusion may indicate a more reduced magma system in this intrusion relative to the other three intrusions.

Moreover, a previous study found that the Mn content in magmatic apatite can be used to estimate the oxygen fugacity of a magmatic system (Miles et al. 2014). The calculated results (Table 1) are based on an equation proposed by Miles et al. (2014) that the Chaoshan intrusion formed from a relatively reduced magmatic system (ΔFMQ+0.1), while the Hucun, Dongguashan, and Xinwuli intrusions formed from relatively more oxidized magmatic systems (>ΔFMQ+3).

To independently verify these aforementioned findings from apatite redox proxies, we have estimated the magmatic oxygen fugacity using zircon Ce data. The data show that the calculated zircon Ce^{4+}/Ce^{3+} ratios for the Chaoshan intrusion are lower than that for the Dongguashan, Xinwuli, and Hucun intrusions. The zircon data also indicate less oxidized condition for the Chaoshan magmatic system than the other three magmatic systems, consistent with the results from apatite (Fig. 8e).

The results from this study indicate that the magma leading to Au mineralization is less oxidized than the magma associated with Cu mineralization. One of the underlying reasons is that the solubility of Au in magma is related to the amount of reduced S (S^{2-}) in the magma, which in turn is related to the oxygen fugacity of the magma (Zajacz et al. 2012). Au can be easily dissolved as a bisulfide complex [such as Au-S-O, AuHS, Au_2S_3, $AuFeS_2$, or AuS(K/Na)] in relatively reduced magma, but it is more difficult to be dissolved in the relatively more oxidized magma (>ΔNNO+1) because under such more oxidized conditions it tends to occur as less soluble species such as metallic Au or AuO_2 (Botcharnikov et al. 2011; Jégo and Pichavant 2012; Zajacz et al. 2012). Several experiments have also demonstrated that the solubility of Au in magma rapidly decreases when oxygen fugacity exceeds ΔFMQ+1, whereas the solubility of Cu continues to increase (Bell et al. 2011; Botcharnikov et al. 2011; Jégo and Pichavant 2012; Zajacz et al. 2012; Li and Audétat 2013). Among the four selected intrusions, Au could be more abundant in the parental magma for the Chaoshan intrusion because the magma was less oxidized (ΔFMQ+0.1) and could dissolve more Au for the later hydrothermal mineralization, whereas Au could be barren in the parental magmas for the other three intrusions (Dongguashan, Hucun, and Xinwuli) because their parental magmas were highly oxidized (>ΔFMQ+3). This may explain the different metallogenic affinities for the different intrusions from this study.

Magma compositions

Volatile components. During magma solidification, volatile components such as F, Cl, H_2O, and S would change in the melt due to crystallization and fluid exsolution or degassing. Hence, the whole-rock composition cannot representatively record the initial volatile contents in magma. Fluid saturation and exsolution may occur at the early stages of magma differentiation in the magma with a high initial water content such as ore-forming magma (usually >4%) (Zhu et al. 2018). This prevents the metal loss caused by crystallization of minerals and facilitates metal partitioning into the hydrothermal fluid (Cline and Bodnar 1991). The parental magma for a porphyry Cu deposit could attain massive fluid exsolution during hornblende crystallization (Li et al. 2018). Therefore, hornblende and biotite may not track the initial halogen compositions of magma if they crystallize after massive fluid exsolution. In some dioritic magmatic systems, such as those from this study, apatite can crystallize earlier than hornblende and biotite, as evidenced by the textures (Fig. 3). In these cases, apatite can be used to evaluate the initial halogen and sulfur compositions of the magma (e.g., Boyce et al. 2010; Elkins-Tanton and Grove 2011).

Our data show that apatite in the Chaoshan intrusion has higher Cl and SO_3 contents but lower F/Cl ratio than apatite in the Hucun, Dongguashan, and Xinwuli intrusions (Fig. 9). The S contents of the parental magmas for these intrusions were estimated using the apatite/melt partition coefficients of Peng et al. (1997) and Parat et al. (2011), and the Cl and F abundances in the magmas were calculated using the apatite/melt partition coefficients of Parat et al. (2011). The results (Table 1) indicate that the Au-mineralized magma contains more Cl and S and less F than the Cu-mineralized magmas. The solubility of Cu is influenced only slightly by the presence of S and Cl because the dominant Cu species in the melt is $CuO_{0.5}$ (Zajacz et al. 2012). In contrast, the solubility of Au increases significantly with increasing S and Cl contents in the melt (Botcharnikov et al. 2011; Zajacz et al. 2012). Considering this different effect of S and Cl on the solubility of Cu and Au in the melt, the enrichment of magmatic S and Cl plays a more important role in the accumulation of sufficient Au in an evolving melt for hydrothermal mineralization. The higher F contents of apatite in these three Cu-mineralized intrusions relative to the Au-mineralized intrusion might be attributed to the input of more crustal components into the parental magmas of the Cu-mineralized intrusions. This is supported by the apatite Sr-Nd isotope (discussed below). Also, the parental magma of the Xinwuli intrusion shows lower Cl and S contents than that of the Hucun and Dongguashan intrusions.

It is generally accepted that Cl shows a strong preference for

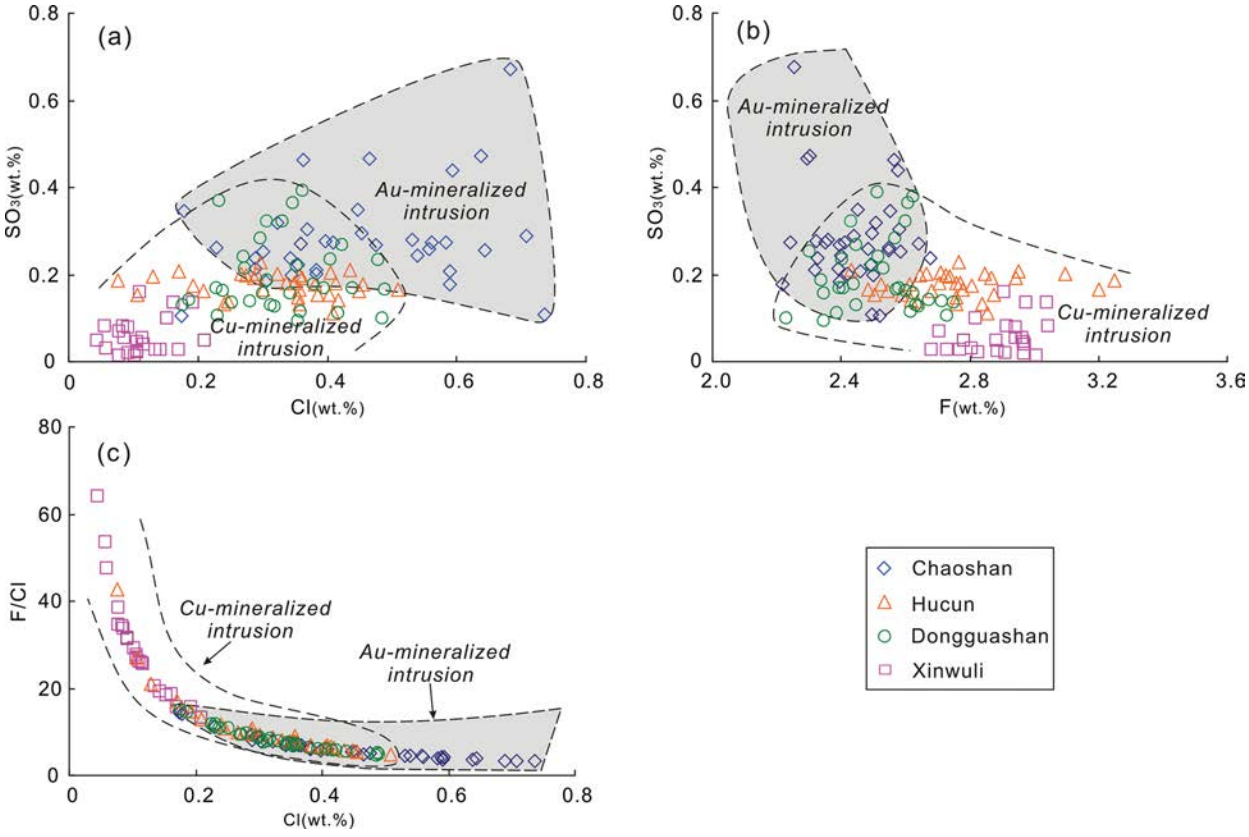

Figure 9. Plots of Cl vs. SO_3, F vs. SO_3, and Cl vs. F/Cl in apatite from the selected intrusions.

aqueous solutions relative to F (Candela 1986; Boudreau and Kruger 1990). Hydrothermal fluid exsolution can inevitably result in the depletion of Cl relative to F in the coexisting melt. Therefore, an increase in the F/Cl ratio of apatite may be indicative of continuous exsolution of Cl-bearing fluid from magma during apatite crystallization (e.g., Huang et al. 2019). Moreover, crystallization of feldspar will decrease Sr in the residual melt (Bedard 2006). During this process, apatite crystallizing late will have a lower Sr content than that crystallizing earlier. This decreased Sr content closely corresponds to the elevated F/Cl ratios in some apatite crystals, which may be due to Cl-bearing fluid exsolution during progressive crystallization of apatite and feldspar (Fig. 10a). But the degree of fluid exsolution is likely limited as fluid inclusions in apatite are rare. Furthermore, if a large amount of Cl-bearing fluids escaped from magma during apatite crystallization, the mole fractions of hydroxylapatite and chlorapatite in apatite would decrease together, which is not indicated by the data (Fig. 10b).

Metal fertility. Whole-rock samples from the host intrusions of porphyry and skarn-type Cu deposits commonly contain minor amounts of disseminated hydrothermal chalcopyrite and bornite. As a result, the Cu contents in whole rocks tend to be higher than those in the parental magmas. Thus, the metal contents in some mineral structures are a better proxy to track the parental magma composition. Apatite may contain Cu through the substitution of Ca^{2+} by Cu^{2+} (Wang et al. 2016). Although the Cu partition coefficient between apatite and melt remains uncertain, the different ionic radius between Cu^{2+} and Ca^{2+} and the low content of Cu in natural apatite indicates that Cu is likely incompatible in the apatite structure. This incompatibility of Cu signifies that apatite crystallizing at any stage of magma evolution is unable to scavenge a significant fraction of Cu from the melt. However, the contents of Cu in some natural apatite crystals are still high enough to be measured by LA-ICP-MS, providing a useful indicator for Cu fertility in the parental magma.

It is widely accepted that the crystallization of major rock-forming minerals such as hornblende, pyroxene, feldspar, and biotite do not remove Cu from the parental magma because Cu is highly incompatible in the mineral structures (Bedard 2006; Le Roux et al. 2015; Hsu et al. 2017; Liu et al. 2015). However, the Cu content in melt and apatite could be strongly controlled by the crystallization of Cu-bearing sulfides or the exsolution of Cu-bearing fluids during apatite crystallization. Crystallization of magmatic sulfides directly from magma will result in a significant decrease of Cu and S in the residual magma because Cu can be sequestered by many sulfide phases (Jugo et al. 1999). The exsolution of Cl-rich fluids from magma will reduce the amount of Cu in the magma because Cu can strongly partition into the fluids as Cl-complexes (Candela and Holland 1984; Williams et al. 1995; Webster 2004). It is currently accepted though that direct saturation of sulfide from magma is not favorable for Cu and Au mineralization (Richards 2015; Sun et al. 2015). In fact, sulfide saturation may occur in relatively reduced magmas but not in highly oxidized magmas (Jugo et al. 2005). For this

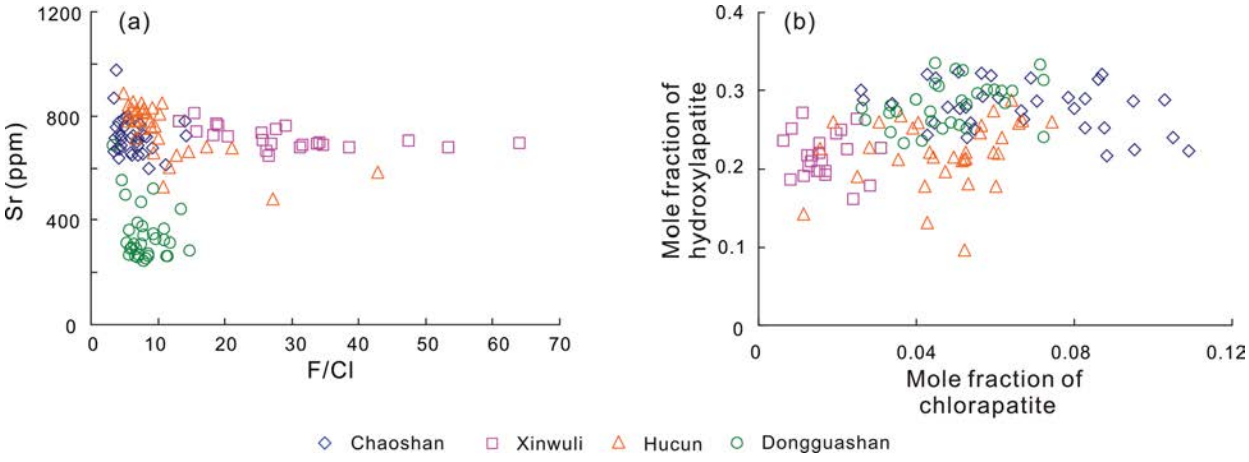

Figure 10. Plots of F/Cl vs. Sr (**a**) and mole fraction of chloraptite vs. hydroxylapatite (**b**) in apatite from the selected intrusions

reason, magmatic sulfides (e.g., pyrite and chalcopyrite) are mainly found in the host rocks of some reduced-type porphyry Cu deposits such as the San Anto (Mexico), Mamut (Malaysia), and San Jorge (Argentina) deposits (f_{O_2} < FMQ; Rowins 2000). The four intrusions we have studied clearly formed from more oxidized magma (f_{O_2} > FMQ). The concentrations of S in the parental magmas for these four intrusions, estimated based on apatite S contents (Table 1), are all lower than the value required for pyrite saturation (~1500 ppm) (Moune et al. 2009) and the S solubility in andesitic and rhyolitic melt (~1000 ppm) (Clemente et al. 2004). Sulfide melt inclusions are absent in these intrusions, which may be partly attributed to high-magmatic oxygen fugacity. Experimental results have shown that S almost exists in the form of S^{6+} in the oxidized magma (f_{O_2} > FMQ+2.0) (Jugo et al. 2005). Based on these conditions, we do not expect that there was major magmatic sulfide saturation in the magma types investigated in this study. If a large amount of Cu was extracted by a Cl-bearing fluid during apatite crystallization from the parental magmas for these intrusions, a reduced Cu content and similarly decreased Cl content in apatite would be expected. But such correlation is not found (Fig. 11a), implying that the potential large-scale hydrothermal fluid exsolution mainly occurred after apatite crystallization, and thus the studied apatite can be used to track the initial Cu contents in the parental magmas.

The contents of Cu in apatite from the Cu-mineralized intrusions are dramatically different (Figs. 11a and 11b). Apatite from the Xinwuli intrusion has a Cu content ten times higher than apatite from the other two intrusions (Hucun and Dongguashan). The contents of Cu in apatite from the Hucun and Dongguashan intrusions are as low as that from the Chaoshan intrusion, which is not related to any Cu mineralization. The reason for the contrasting Cu contents in apatite from the three Cu-mineralized intrusion is elusive, but one possibility is a different magma source for the different intrusions, each source with different Cu abundances. Cu-rich magma is considered to be a prerequisite for the formation of porphyry- and skarn-type Cu deposits by some researchers (e.g., Halter et al. 2005; Core et al. 2006; Stern et al. 2007; Richards 2009). The results from this study, as well as those from the study of the Bingham deposits (Zhang and Audétat 2017), indicate that such requirement is not universal. We believe that fluid compositions can play a prominent part in Cu mineralization. The fluids derived from the relatively Cl-rich

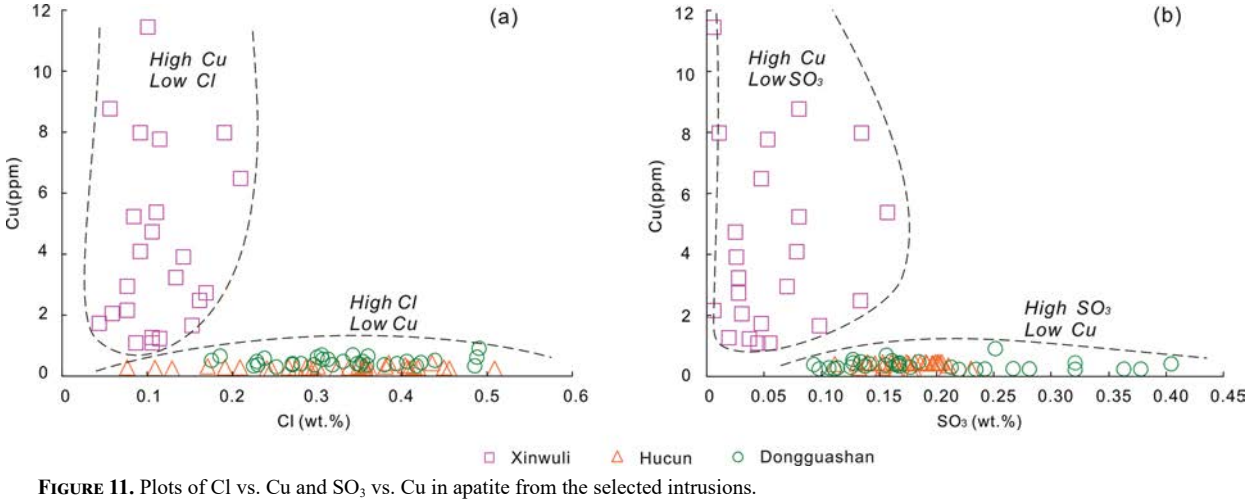

Figure 11. Plots of Cl vs. Cu and SO_3 vs. Cu in apatite from the selected intrusions.

magmas of the Hucun and Dongguashan intrusions are likely to contain more high-salinity fluids and thus can transport more Cu as Cl-complexes. This is conducive to the extraction of Cu into the hydrothermal fluid and can lead to Cu mineralization even if the parental magma is not particularly enriched in Cu.

Mantle and crustal components in the parental magmas

As mentioned above, apatite major and trace elements reveal significant differences in the redox conditions and chemical compositions between Au-mineralized and Cu-mineralized magmatic systems. These differences may be partly related to the mixing of magmas with different proportions of the crust-derived and mantle-derived components. Previous studies have shown that F is high in the crust (Aoki et al. 1981; Gundmundur et al. 1986). Thus, we envisage that higher F content in apatite from the intrusions related to Cu mineralization relative to that in apatite associated with Au mineralization might result from the higher contribution of the crust-derived components to the parental magmas of these intrusions. The whole-rock Sr-Nd isotope data for the igneous rocks in the Tongling region show that pyroxene diorite such as that of the Chaoshan intrusion generally have lower $(^{87}Sr/^{86}Sr)_i$ ratios and higher εNd(t) values than granodiorite and quartz diorite such as those in the Hucun, Dongguashan, and Xinwuli intrusions (Xie 2008). However, owing to the possible effect from weathering and alteration on whole-rock Sr-Nd isotope data, more evidence is needed to reach this conclusion. Recently, the values of in situ apatite $^{87}Sr/^{86}Sr$ and $^{143}Nd/^{144}Nd$ have been accurately detected by LA-MC-ICP-MS (Yang et al. 2014). The advantage of Sr-Nd isotope in apatite as an effective reflection of that in the parental magma is that the early crystallization of apatite could largely avoid the possible isotope fractionation caused by the late crystallization of other minerals. Our apatite results show higher εNd(t) values and lower initial $(^{87}Sr/^{86}Sr)_i$ ratios for the Chaoshan intrusion than the other three intrusions (Fig. 12). The Sr-Nd isotope data are consistent with the interpretation that the parental magma of the Au-mineralized Chaoshan intrusion contains higher amount of mantle-derived materials than those of the other three Cu-mineralized intrusions.

The finding that magma with a larger mantle component is favorable for Au mineralization might be ascribed to Au fertilization in the metasomatized enriched lithospheric mantle. Previous studies have shown that the metasomatized enriched lithospheric mantle, such as that in North China and Papua New Guinea, could be enriched in Au (Griffin et al. 2013; Saunders et al. 2018; McInnes et al. 1999). The Au content in the mantle xenoliths collected nearly 300 km away from the Tongling ore district can exceed 6.0 ppb (He et al. 2004), which is higher than the average Au abundance in the continental crust (1.5–3.0 ppb, Taylor and McLennan 1995; Rudnick and Gao 2003). Alternatively, a relatively Si-poor magma (SiO_2 < 60 wt%) due to the mixing with abundant mantle materials will effectively suppress the early crystallization of magnetite and sulfide (Jenner et al. 2010). This is more critical for the mineralization of Au than that of Cu by avoiding the early loss of ore-forming metal from the magma, owing to the higher solid/melt partition coefficient for Au than Cu (Peach et al. 1990; Li and Audétat 2012; Patten et al. 2013; Mungall and Brenan 2014). Nevertheless, there is no evidence for the early saturation of sulfide and magnetite in causative magmas of the Cu-mineralized intrusions investigated. Therefore, we favor the addition of different amounts of mantle-derived materials as the reason for the different metallogeny.

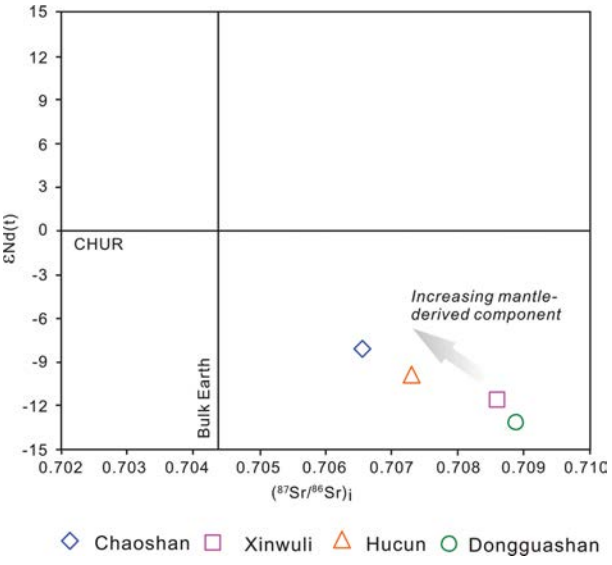

Figure 12. Plots of average $(^{87}Sr/^{88}Sr)_i$ vs. average εNd(t) in apatite from the selected intrusions.

Implications

The results of this study demonstrate that apatite is a good petrogenetic and metallogenic indicator. V-Mn concentrations and Ce/La ratio in apatite can be used to estimate the oxidation states of the parental magma. The concentrations of F, Cl, S, and Cu in apatite can be used to track the volatile compositions and metal fertility of the magma. The apatite Sr-Nd isotopes can be used to evaluate the contributions of crustal and mantle components in the ore-forming magma. The variations of the above proxies in apatite from the selected four intrusions indicate that the magma related to Au mineralization is less oxidized and has higher S and Cl contents plus lower F content than the magma associated with Cu mineralization. We attribute these differences to the possibility that the magma of the Au mineralized system contains higher amounts of mantle-derived components than magma of the Cu mineralized systems, as inferred from the apatite Sr-Nd isotopes. We have also found that apatite from the Cu-mineralized intrusions can have high- and low-Cu contents with a difference up to ten times, implying that Cu-rich magma is not the prerequisite of porphyry Cu ore formation. Finally, the results from this study indicate that apatite is better than whole rocks to track the compositions of halogen and some trace elements and metals in the parental magma.

Acknowledgments

We thank Yan-Wen Tang for his assistance in apatite and zircon trace element analysis by LA-ICP-MS, Wen-Qin Zheng and Xiang Li for their support in apatite chemical analysis by EPMA, You-Wei Chen for his help in apatite Sr-Nd isotopes analysis by LA-MC-ICP-MS and Jing Hu and Shu-Qin Yang for their assistance in the whole-rock chemical analysis by XRF and ICP-MS. We thank the Associate Editor Antonio Acosta-Vigil, Thomas Ulrich, and an anonymous reviewer for constructive reviews. We are grateful to Chusi Li of Indiana University and Thomas Ulrich for their help in manuscript revision.

Funding

This study was supported by the Strategic Priority Research Program (B) of the Chinese Academy of Sciences (XDB18000000), "Light of West China" Program of Chinese Academy of Sciences, the National Natural Science Foundation of China (Grant 41703050), and the CAS/SAFEA International Partnership Program for Creative Research Teams (Intraplate Mineralization Research Team; KZZD-EW-TZ-20).

References cited

Acosta-Vigil, A., London, D., Morgan, G.B. VI, and Dewers, T.A. (2003) Solubility of excess alumina in hydrous granitic melts in equilibrium with peraluminous minerals at 700–800 °C and 200 MPa, and applications of the aluminum saturation index. Contributions to Mineralogy and Petrology, 146, 100–119.

Aoki, K., Ishiwaka, K., and Kanisawa, S. (1981) Fluorine geochemistry of basaltic rocks from continental and oceanic regions and petrogenetic application. Contributions to Mineralogy and Petrology, 78, 53–59.

Ayers, J.C., and Watson, E.B. (1991) Solubility of apatite, monazite, zircon, and rutile in supercritical aqueous fluids with implications for subduction zone geochemistry. Philosophical Transactions of the Royal Society of London, A, 335, 365–375.

Ballard, J.R., Palin, J.M., and Campbell, I.H. (2002) Relative oxidation states of magmas inferred from Ce(IV)/Ce(III) in zircon: application to porphyry copper deposits of Northern Chile. Contributions to Mineralogy and Petrology, 144, 347–364.

Bedard, J.H. (2006) Trace element partitioning in plagioclase feldspar. Geochimica et Cosmochimica Acta, 70, 3717–3742.

Bell, A.S., Simon, A., and Guillong, M. (2011) Gold solubility in oxidized and reduced, water-saturated mafic melt. Geochimica et Cosmochimica Acta, 75, 1718–1732.

Belousova, E.A., Walters, S., Griffin, W.L., and O'Reilly, S.Y. (2001) Trace-element signatures of apatites in granitoids from the Mt. Isa Inlier, northwestern Queensland. Australian Journal of Earth Sciences, 48, 603–619.

Belousova, E.A., Griffin, W.L., O'Reilly, S.Y., and Fisher, N.I. (2002) Apatite as an indicator mineral for mineral exploration: Trace-element composition and their relationship to host rock type. Journal of Geochemical Exploration, 76, 45–69.

Bi, X.W., Cornell, D.H., and Hu, R.Z. (2002) REE composition of primary and altered feldspar from the mineralized alteration zone of alkali-rich intrusive rocks, Western Yunnan Province, China. Ore Geology Reviews, 19, 69–78.

Bi, X.W., Hu, R.Z., Hanley, J.J., Mungall, J., Peng, J.T., Shang, L.B., Wu, K.X., Suang, Y., Li, H.L., and Hu, X.Y. (2009) Crystallisation conditions (T, P, f_{O_2}) from mineral chemistry of Cu- and Au-mineralised alkaline intrusions in the Red River-Jinshajiang alkaline igneous belt, western Yunnan Province, China. Mineralogy and Petrology, 96, 43–58.

Boechat, C.B., Terra, J., Eon, J.G., Ellis, D.E., and Rossi, A.M. (2003) Reduction by hydrogen of vanadium in vanadate apatite solid solutions. Physical Chemistry Chemical Physics, 5, 4290–4298.

Botcharnikov, R.E., Linnen, R.L., Wilke, M., Holtz, F., Jugo, P.J., and Berndt, J. (2011) High gold concentrations in sulphide-bearing magma under oxidizing conditions. Nature Geoscience, 4, 112–115.

Boudreau, A.E., and Kruger, F.J. (1990) Variation in the composition of apatite through the Merensky cyclic unit in the Western Bushveld Complex. Economic Geology, 85, 737–745.

Bouzari, F., Hart, C.J.R., Bissig, T., and Barker, S. (2016) Hydrothermal alteration revealed by apatite luminescence and chemistry: A potential indicator mineral for exploring covered porphyry copper deposits. Economic Geology, 111, 1397–1410.

Boyce, J.W., Liu, Y., Rossman, G.R., Guan, Y.B., Eiler, J.M., Stolper, E.M., and Taylor, L.A. (2010) Lunar apatite with terrestrial volatile abundances. Nature, 466, 466–470.

Buick, I.S., Hermann, J., Maas, R., and Gibson, R.L. (2007) The timing of subsolidus hydrothermal alteration in the central zone, Limpopo Belt (South Africa): Constraints from titanite U-Pb geochronology and REE partitioning. Lithos, 98, 97–117.

Candela, P.A. (1986) Toward a thermodynamic model for the halogens in magmatic systems: An application to melt-vapor-apatite equilibria. Chemical Geology, 57, 289–301.

Candela, P.A., and Holland, H.D. (1984) The partitioning of copper and molybdenum between silicate melts and aqueous fluids. Geochimica et Cosmochimica Acta, 48, 373–388.

Cao, M.J., Li, G.M., Qin, K.Z., Seitmuratova, E.Y., and Liu, Y.S. (2012) Major and trace element characteristics of apatites in granitoids from Central Kazakhstan: implications for petrogenesis and mineralization. Resource Geology, 62, 63–83.

Cao, Y., Zheng, Z., Du, Y., Gao, F., Qin, X., Yang, H., Lu, Y., and Du, Y. (2017) Ore geology and fluid inclusions of the Hucunnan deposit, Tongling, Eastern China: Implications for the separation of copper and molybdenum in skarn deposits. Ore Geology Reviews, 83, 152–173.

Chu, M.F., Wang, K.L., Griffin, W.L., Chung, S.L., O'Reilly, S.Y., Pearson, N.J., and Iizuka, Y. (2009) Apatite composition: Tracing petrogenetic processes in Transhimalayan granitoids. Journal of Petrology, 50, 1829–1855.

Clemente, B., Scaillet, B., and Pichavant, M. (2004) The solubility of sulphur in hydrous rhyolitic melts. Journal of Petrology, 45, 2171–2196.

Cline, J.S., and Bodnar, R.J. (1991) Can economic porphyry copper mineralization be generated by a typical calc-alkaline melt? Journal of Geophysical Research, 96, 8113–8126.

Cooke, D.R., Hollings, P., and Walshe, J. (2005) Giant porphyry deposits: Characteristics, distribution, and tectonic controls. Economic Geology, 100, 801–818.

Core, D.P., Kesler, S.E., and Essene, E.J. (2006) Unusually Cu-rich magmas associated with giant porphyry copper deposits: Evidence from Bingham, Utah. Geology, 34, 41–44.

Creaser, R.A., and Gray, C.M. (1992) Preserved initial $^{87}Sr/^{86}Sr$ in apatite from altered felsic igneous rocks: a case study from Middle Proterozoic of South Australia. Geochimica et Cosmochimica Acta, 56, 2789–2795.

Defant, M.J., and Drummond, M.S. (1990) Derivation of some modern arc magmas by melting of young subducted lithosphere. Nature, 347, 662–665.

Deng, J., Wang, Q.F., Xiao, C.H., Yang, L.Q., Liu, H., Gong, Q.J., and Zhang, J. (2011) Tectonic-magmatic-metallogenic system, Tongling ore cluster region, Anhui Province, China. International Geology Review, 53, 449–476.

Ding, T., Ma, D.S., Lu, J.J., and Zhang, R.Q. (2015) Apatite in granitoids related to polymetallic mineral deposits in southeastern Hunan Province, Shi-Hang zone, China: Implications for petrogenesis and metallogenesis. Ore Geology Reviews, 69, 104–117.

Drake, M.J. (1975) Oxidation state of europium as an indicator of oxygen fugacity. Geochimica et Cosmochimica Acta, 39, 55–64.

Ekstrom, T.K. (1972) The distribution of fluorine among some coexisting minerals. Contributions to Mineralogy and Petrology, 34, 192–200.

Elkins-Tanton, L.T., and Grove, T.L. (2011) Water (hydrogen) in the lunar mantle: Results from petrology and magma ocean modeling. Earth and Planetary Science Letters, 307, 173–179.

Ferry, J.M., and Watson, E.B. (2007) New thermodynamic models and revised calibrations for the Ti-in-zircon and Zr-in-rutile thermometers. Contributions to Mineralogy and Petrology, 154, 429–437.

Gao, J.F., and Zhou, M.F. (2013) Generation and evolution of siliceous high magnesium basaltic magmas in the formation of the Permian Huangshandong intrusion (Xinjiang, NW China). Lithos, 162, 128–139.

Goldoff, B., Webster, J.D., and Harlov, D.E. (2012) Characterization of fluor-chlorapatites by electron probe microanalysis with a focus on time-dependent intensity variation of halogens. American Mineralogist, 97, 1103–1115.

Griffin, W.L., Begg, G.C., and O'Reilly, S.Y. (2013) Continental-root control on the genesis of magmatic ore deposits. Nature Geoscience, 6, 905–910.

Gundmundur, E., Sigvaldson, E., and Oskarsson, N. (1986) Fluorine in basalts from Iceland. Contributions to Mineralogy and Petrology, 94, 263–271.

Halter, W.E., Heinrich, C.A., and Pettke, T. (2005) Magma evolution and the formation of porphyry Cu-Au ore fluids: Evidence from silicate and sulfide melt inclusions. Mineralium Deposita, 39, 845–863.

Harrison, T.M., and Watson, E.B. (1984) The behavior of apatite during crustal anatexis: Equilibrium and kinetic consideration. Geochimica et Cosmochimica Acta, 48, 1467–1477.

He, Y., Dong, Z.X., Yue, K.F., Zhang, Z.J., Chen, J.W., and Wang, X. (2004) Content of mantle-derived xenoliths in Eastern China and its metallogenic significance. Geological Review, 50, 418–425.

Henrichs, I.A., O'Sullivan, G., Chew, D.M., Mark, C., Babechuk, M.G., McKenna, C., and Emo, R. (2018) The trace element and U-Pb systematics of metamorphic apatite. Chemical Geology, 483, 218–238.

Hou, Z.Q., Zeng, P.S., Gao, Y.F., Du, A.D., and Fu, D.M. (2006) Himalayan Cu-Mo-Au mineralization in the eastern Indo-Asian collision zone: Constraints from Re-Os dating of molybdenite. Mineralium Deposita, 41, 33–45.

Hsu, Y.J., Zajacz, Z., Ulmer, P., and Heinrich, C.A. (2017) Copper partitioning between silicate melts and amphibole: Experimental insight into magma evolution leading to porphyry copper ore formation. Chemical Geology, 448, 151–163.

Huang, M.L., Bi, X.W., Richards, J.P., Hu, R.Z., Xu, L.L., Gao, J.F., Zhu, J.J., and Zhang, X.C. (2019) High water contents of magmas and extensive fluid exsolution during the formation of the Yulong porphyry Cu-Mo deposit, eastern Tibet. Journal of Asian Earth Sciences, 176, 168–183.

Imai, A. (2002) Metallogenesis of porphyry Cu deposits of the western Luzon arc, Philippines: K-Ar ages, SO_3 contents of microphenocrystic apatite and significance of intrusive rocks. Resource Geology, 52, 147–161.

——— (2004) Variation of Cl and SO_3 contents of microphenocrystic apatite in intermediate to silicic igneous rocks of Cenozoic Japanese island arcs: implications for porphyry Cu metallogenesis in the Western Pacific Island arcs. Resource Geology, 54, 357–372.

Irvine, I.N., and Baragar, W.R.A. (1971) A guide to the chemical classification of the common volcanic rocks. Canadian Journal of Earth Sciences, 8, 523–548.

Isnard, H., Brennetot, R., Caussignac, C., Caussignac, N., and Chartier, F. (2005) Investigations for determination of Gd and Sm isotopic compositions in spent nuclear fuels samples by MC ICPMS. International Journal of Mass Spectrometry, 246, 66–73.

Jahnke, R.A. (1984) The synthesis and solubility of carbonate fluorapatite. American Journal of Science, 284, 58–78.

Jégo, S., and Pichavant, M. (2012) Gold solubility in arc magmas: Experimental determination of the effect of sulfur at 1000 °C and 0.4 GPa. Geochimica et Cosmochimica Acta, 84, 560–592.
Jenner, F.E., O'Neill, H.St.C., Arculus, R.J., and Mavrogenes, J.A. (2010) The Magnetite crisis in the evolution of arc-related magmas and the initial concentration of Au, Ag and Cu. Journal of Petrology, 51, 2445–2464.
Johnston, A.D., and Schwab, B.E. (2004) Constraints on clinopyroxene/melt partitioning of REE, Rb, Sr, Ti, Cr, Zr, and Nb during mantle melting: First insights from direct peridotite melting experiments at 1.0 GPa. Geochimica et Cosmochimica Acta, 68, 4949–4962.
Jugo, P.J., Candela, P.A., and Piccoli, P.M. (1999) Magmatic sulfides and Au:Cu ratios in porphyry deposits: An experimental study of copper and gold partitioning at 850 °C, 100 MPa in a haplogranitic melt-pyrrhotite-intermediate solid solution-gold metal assemblage, at gas saturation. Lithos, 46, 573–589.
Jugo, P.J., Luth, R.W., and Richards, J.P. (2005) Experimental data on the speciation of sulfur as a function of oxygen fugacity in basaltic melts. Geochimica et Cosmochimica Acta, 69, 497–503.
Le Roux, V., Dasgupta, R., and Lee, C.T.A. (2015) Recommended mineral-melt partition coefficients for FRTEs (Cu), Ga, and Ge during mantle melting. American Mineralogist, 100, 2533–2544.
Lerchbaumer, L., and Audétat, A. (2013) The metal content of silicate melts and aqueous fluids in subeconomically Mo mineralized granites: implications for porphyry Mo genesis. Economic Geology, 108, 987–1013.
Li, Y., and Audétat, A. (2012) Partitioning of V, Mn, Co, Ni, Cu, Zn, As, Mo, Ag, Sn, Sb, W, Au, Pb, and Bi between sulfide phases and hydrous basanite melt at upper mantle conditions. Earth and Planetary Science Letters, 355-356, 327–340.
——— (2013) Gold solubility and partitioning between sulfide liquid, monosulfide solid solution and hydrous mantle melts: Implications for the formation of Au-rich magmas and crust–mantle differentiation. Geochimica et Cosmochimica Acta, 118, 247–262.
Li, Z.X., and Li, X.H. (2007) Formation of the 1300-km-wide intracontinental orogen and postorogenic magmatic province in Mesozoic South China: A flat-slab subduction model. Geology, 35, 179–182.
Li, S., Yang, X.Y., Huang, Y., and Sun, W.D. (2014) Petrogenesis and mineralization of the Fenghuangshan skarn Cu-Au deposit, Tongling ore cluster field, Lower Yangtze metallogenic belt. Ore Geology Reviews, 58, 148–162.
Li, J.X., Qin, K.Z., Li, G.M., Evans, N.J., Zhao, J.X., Yue, Y.H., and Xie, J. (2018) Volatile variations in magmas related to porphyry Cu-Au deposits: Insights from amphibole geochemistry, Duolong district, central Tibet. Ore Geology Reviews, 95, 649–662.
Liu, Y.S., Hu, Z.C., Gao, S., Gunther, D., Xu, J., Gao, C.G., and Chen, H.H. (2008) In situ analysis of major and trace elements of anhydrous minerals by LA-ICP-MS without applying an internal standard. Chemical Geology, 257, 34–43.
Liu, X., Xiong, X., Audétat, A., and Li, Y. (2015) Partitioning of Cu between mafic minerals, Fe-Ti oxides and intermediate to felsic melts. Geochimica et Cosmochimica Acta, 151, 86–102.
Liu, Z.F., Shao, Y.J., Wang, C., and Liu, Q.Q. (2019) Genesis of the Dongguashan skarn Cu-(Au) deposit in Tongling, Eastern China: Evidence from fluid inclusions and H-O-S-Pb isotopes. Ore Geology Reviews, 104, 462–476.
London, D., Wolf, M.B., Morgan, G.B. VI, and Garrido, M.G. (1999) Experimental silicate-phosphate equilibria in peraluminous granitic magmas, with a case study of Albuquerque batholith at Tres Arroyos, Badajoz, Spain. Journal of Petrology, 40, 215–240.
Lu, S.M., Xu, X.C., Xie, Q.Q., Lou, J.W., Chu, G.Z., and Xiong, Y.P. (2007) Chemical and stable isotope geochemical characteristics of ore-forming fluid of the Shizishan copper and gold ore-field, Tongling, China. Acta Petrologica Sinica, 23, 177–184 (in Chinese with English abstract).
Mallmann, G., and O'Neill, H.St.C. (2009) The crystal/melt partitioning of V during mantle melting as a function of oxygen fugacity compared with some other elements (Al, P, Ca,Sc, Ti, Cr, Fe, Ga,Y, Zr and Nb). Journal of Petrology, 50, 1765–1794.
Maniar, P.D., and Piccoli, P.M. (1989) Tectonic discrimination of granitoids. Geological Society of America Bulletin, 101, 635 –643.
Mao, M., Rukhlov, A.S., Rowins, S.M., Spence, J., and Coogan, L.A. (2016) Apatite trace element compositions: a robust new tool for mineral exploration. Economic Geology, 111, 1187–1222.
McInnes, B.I., McBride, J.S., Evans, N.J., Lambert, D.D., and Andrew, A.S. (1999) Osmium isotope constraints on ore metal recycling in subduction zones. Science, 286, 512–516.
Meinert, L.D., Dipple, G.M., and Nicolescu, S. (2005) World skarn deposits. Economic Geology, 100th Anniversary Volume, 299–336.
Miles, A.J., Graham, C.M., Hawkesworth, C.J., Gillespie, M.R., Hinton, R.W., Bromiley, G.D., and EMMAC. (2014) Apatite: A new redox proxy for silicic magmas? Geochimica et Cosmochimica Acta, 132, 101–119.
Mercer, C.N., Watts, K.E., and Gross, J. (2020) Apatite trace element geochemistry and cathodoluminescent textures—A comparison between regional magmatism and the Pea Ridge IOAREE and Boss IOCG deposits, southeastern Missouri iron metallogenic province, U.S.A. Ore Geology Reviews, 116, 103129.
Moune, S., Holtz, F., and Botcharnikov, R.E. (2009) Sulphur solubility in andesitic to basaltic melts: Implications for Hekla volcano. Contributions to Mineralogy and Petrology, 157, 691–707.
Mungall, J.E., and Brenan, J.M. (2014) Partitioning of platinum-group elements and Au between sulfide liquid and basalt and the origins of mantle-crust fractionation of the chalcophile elements. Geochimica et Cosmochimica Acta, 125, 265–289.
Myers, J., and Eugster, H.P. (1983) The system Fe-Si-O: Oxygen buffer calibrations to 1,500K. Contributions to Mineralogy and Petrology, 82, 75–90.
Nardi, L.V.S., Formoso, M.L.L., Müller, I.F., Fontana, E., Jarvis, K., and Lamarão, C. (2013) Zircon/rock partition coefficients of REEs, Y, Th, U, Nb, and Ta in granitic rocks: Uses for provenance and mineral exploration purposes. Chemical Geology, 335, 1–7.
Palma, G., Barra, F., Reich, M., Valencia, V., Simon, A.C., Vervoort, J., Leisen, M., and Romero, R. (2019) Halogens, trace element concentrations, and Sr-Nd isotopes in apatite from iron oxide-apatite (IOA) deposits in the Chilean iron belt: Evidence for magmatic and hydrothermal stages of mineralization. Geochimica et Cosmochimica Acta, 246, 515–540.
Pan, Y., and Dong, P. (1999) The lower Changjiang (Yangtze River) metallogenic belt, eastern central China: Intrusion- and wall rock-hosted Cu-Fe-Au, Mo, Zn, Pb, Ag deposits. Ore Geology Reviews, 15, 177–242.
Pan, Y., and Fleet, M.E. (2002) Compositions of the apatite group minerals: substitution mechanisms and controlling factors. Reviews in Mineralogy and Geochemistry, 48, 13–49.
Parat, F., Holtz, F., and Klügel, A. (2011) S-rich apatite-hosted glass inclusions in xenoliths from La Palma: Constraints on the volatile partitioning in evolved alkaline magmas. Contributions to Mineralogy and Petrology, 162, 463–478.
Patten, C., Barnes, S.J., Mathez, E.A., and Jenner, F.E. (2013) Partition coefficients of chalcophile elements between sulfide and silicate melts and the early crystallization history of sulfide liquid: LA-ICP-MS analysis of MORB sulfide droplets. Chemical Geology, 358, 170–188.
Peach, C.L., Mathez, E.A., and Keays, R.R. (1990) Sulfide melt-silicate melt distribution coefficients for noble metals and other chalcophile elements as deduced from MORB: Implications for partial melting. Geochimica et Cosmochimica Acta, 54, 3379–3389.
Peng, G., Luhr, J.F., and McGee, J.J. (1997) Factors controlling sulfur concentrations in volcanic apatite. American Mineralogist, 82, 1210–1224.
Piccoli, P.M., and Candela, P.A. (1994) Apatite in felsic rocks: A model for the estimation of initial halogen concentrations in the Bishop Tuff (Long Valley) and Tuolumne intrusive suite (Sierra Nevada batholith) magmas. American Journal of Science, 294, 92–135.
——— (2002) Apatite in igneous systems. Reviews in Mineralogy and Geochemistry, 48, 255–292.
Pichavant, M., Montel, J.M., and Richard, L.R. (1992) Apatite solubility in peraluminous liquids: Experimental data and an extension of the Harrison-Watson model. Geochimica et Cosmochimica Acta, 56, 3855–3861.
Qi, L., Hu, J., and Gregoire, D.C. (2000) Determination of trace elements in granites by inductively coupled plasma mass spectrometry. Talanta, 51, 507–513.
Qian, L., Wang, Y., Xie, J.C., and Sun, W.D. (2019) The Late Mesozoic granodiorite and polymetallic mineralization in southern Anhui Province, China: A perspective from apatite geochemistry. Solid Earth Sciences, 4, 178–189.
Ramos, F.C., Wolff, J.A., and Tollstrup, D.L. (2004) Measuring $^{87}Sr/^{86}Sr$ variations in minerals and groundmass from basalts using LA-MC-ICPMS. Chemical Geology, 211, 135–158.
Richards, J.P. (2009) Postsubduction porphyry Cu-Au and epithermal Au deposits: Products of remelting of subduction-modified lithosphere. Geology, 37, 247–250.
——— (2015) The oxidation state, and sulfur and Cu contents of arc magmas: Implications for metallogeny. Lithos, 233, 27–45.
Richards, J.P., and Şengör, A.M.C. (2017) Did Paleo-Tethyan anoxia kill arc magma fertility for porphyry copper formation? Geology, 45, 591–594.
Rittmann, A. (1957) On the serial character of igneous rocks. Egyptian Journal of Geology, 1, 23–48.
——— (1962) Volcanoes and their Activity. Interscience Publishers, New York.
Rønsbo, J.G. (1989) Coupled substitutions involving REEs and Na and Si in apatites in alkaline rocks from the Ilímaussaq intrusion, South Greenland, and the petrological implications. American Mineralogist, 74, 896–901.
Rowins, S.M. (2000) Reduced porphyry copper-gold deposits: A new variation on an old theme. Geology, 8, 167–180.
Rubatto, D., and Hermann, J. (2007) Experimental zircon/melt and zircon/garnet trace element partitioning and implications for the geochronology of crustal rocks. Chemical Geology, 241, 38–61.
Rudnick, R.L., and Gao, S. (2003) Composition of the continental crust. Treatise on Geochemistry, 3, 1–64.
Saunders, J.E., Pearson, N.J., O'Reilly, S.Y., and Griffin, W.L. (2018) Gold in the mantle: A global assessment of abundance and noredistribution processes. Lithos, 322, 376–391.
Sha, L.K., and Chappell, B.W. (1999) Apatite chemical composition, determined by electron microprobe and laser-ablation inductively coupled plasma mass spectrometry, as a probe into granite petrogenesis. Geochimica et Cosmochimica Acta, 63, 3861–3881.
Shao, Y.J., Peng, S.L., Lai, J.Q., Liu, L.M., Zhang, Y.Z., and Zhang, J.D. (2007)

Identification of two types of mineralized intrusion in the Fenghuangshan copper deposit and analysis of their genesis. Acta Petrologica Sinica, 23, 2471–2482 (in Chinese with English abstract).
Sillitoe, R.H. (2010) Porphyry copper systems. Economic Geology, 105, 3–41.
Stern, C.R., Funk, J.A., Skewes, M.A., and Arévalo, A. (2007) magmatic anhydrite in plutonic rocks at the El Teniente Cu-Mo deposit, Chile, and the role of sulfur- and copper-rich magmas in its formation. Economic Geology, 102, 1335–1344.
Stormer, J.C., Pierson, M.L., and Tacker, R.C. (1993) Variation of F and Cl X-ray intensity due to anisotropic diffusion in apatite during electron microprobe analysis. American Mineralogist, 78, 641–648.
Streck, M.J., and Dilles, J.H. (1998) Sulfur evolution of oxidized arc magmas as recorded in apatite from a porphyry copper batholith. Geology, 26, 523–526.
Sun, S.S., and McDonough, W.F. (1989) Chemical and isotopic systematics of oceanic basalts: Implications for mantle composition and processes. Geological Society Special Publication, 42, 313–345.
Sun, W.D., Ding, X., Hu, Y.H., and Li, X.H. (2007) The golden transformation of the Cretaceous plate subduction in the west Pacific. Earth and Planetary Science Letters, 262, 533–542.
Sun, W.D., Huang, R.F., Li, H., Hu, Y.B., Zhang, C.C., Sun, S.J., Zhang, L.P., Ding, X., Li, C.Y., Zartman, R.E., and Ling, M.X. (2015) Porphyry deposits and oxidized magmas. Ore Geology Reviews, 65, 97–131.
Sun, S.J., Yang, X.Y., Wang, G.J., Sun, W.D., Zhang, H., Li, C.Y., and Ding, X. (2019) In situ elemental and Sr-O isotopic studies on apatite from the Xu-Huai intrusion at the southern margin of the North China Craton: Implications for petrogenesis and metallogeny. Chemical Geology, 510, 200–214.
Taylor, S.R., and McLennan, S.M. (1995) The geochemical evolution of the continental crust. Reviews of Geophysics, 33, 241–265.
Tepper, J.H., and Kuehner, S.M. (1999) Complex zoning in apatite from the Idaho batholith: A record of magma mixing and intracrystalline trace element diffusion. American Mineralogist, 84, 581–595.
Tollari, N., Barnes, S.J., Cox, R.A., and Nabilb, H. (2008) Trace element concentrations in apatites from the Sept-Îles Intrusive Suite, Canada—Implications for the genesis of nelsonites. Chemical Geology, 252, 180–190.
Tu, W. (2014) Characteristics and genesis of the Chaoshan skarn gold deposit, Tongling, Anhui Province. Ph.D. thesis, China University of Geosciences (Beijing) (in Chinese with English abstract).
Wang, Y.B., Liu, D.Y., Zeng, P.S., Yang, Z.S., and Tian, S.H. (2004) SHRIMP U-Pb geochronology of pyroxene diorite in the Chaoshan gold deposit and its geological significance. Acta Geoscientica Sinica, 25, 423–427 (in Chinese with English abstract).
Wang, Q., Wyman, D.A., Xu, J.F., Zhao, Z.H., Jian, P., Xiong, X.L., Bao, Z.W., Li, C.F., and Bai, Z.H. (2006) Petrogenesis of Cretaceous adakitic and shoshonitic igneous rocks in the Luzong area, Anhui Province (eastern China). Implications for geodynamics and Cu-Au mineralization. Lithos, 89, 424–446.
Wang, J.Z., Li, J.W., Zhao, X.F., Ma, C.Q., Qu, W.J., and Du, A.D. (2008a) Re-Os dating of pyrrhotite from the Chaoshan Gold Skarn, Eastern Yangtze Craton, Eastern China. International Geology Review, 50, 392–406.
Wang, J.Z., Li, J.W., Zhao, X.F., Qian, Z.Z., and Ma, C.Q. (2008b) Genesis of the Chaoshan gold deposit and its host intrusion, Tongling area: Constraints from $^{40}Ar/^{39}Ar$ ages and elemental and Sr-Nd-O-C-S isotope geochemistry. Acta Petrologica Sinica, 24, 1875–1888 (in Chinese with English abstract).
Wang, S.W., Zhou, T.F., Yuan, F., Fan, Y., Zhang, L.J., and Song, Y.L. (2015) Petrogenesis of Dongguashan skarn-porphyry Cu-Au deposit related intrusion in the Tongling district, eastern China: Geochronological, mineralogical, geochemical and Hf isotopic evidence. Ore Geology Reviews, 64, 53–70.
Wang, H., Zhang, Y., Chu, Y., Ma, H., Li, Y., Wu, D., Du, B., and Wei, Q. (2016) Disposable competitive-type immunoassay for determination of aflatoxin B1 via detection of copper ions released from Cu-apatite. Talanta, 147, 556–560.
Wang, C.S., Wu, C.L., Zheng, K., Wu, D., Shan, S.F., Li, X., and Gu, Q.D. (2018) Ore-forming ages and sources of metallogenic materials of Fenghuangshan ore field in Tongling. Mineral Deposits, 37, 1195–1216 (in Chinese with English abstract).
Warner, S., Martin, R.F., Abdel-Rahman, A.M., and Doig, R. (1998) Apatite as a monitor of fractionation, degassing, and metamorphism in the Sudbury igneous complex, Ontario. Canadian Mineralogist, 36, 981–999.
Watson, E.B. (1979) Apatite saturation in basic to intermediate magmas. Geophysical Research Letters, 6, 937–940.
——— (1980) Apatite and phosphorus in mantle source regions: an experimental study of apatite/melt equilibria at pressures to 25 kbar. Earth and Planetary Science Letters, 51, 322–335.
Webster, J.D. (2004) The exsolution of magmatic hydrosaline chloride liquids. Chemical Geology, 210, 33–48.
Williams, T.J., Candela, P.A., and Piccoli, P.M. (1995) The partitioning of copper between silicate melts and two-phase aqueous fluids: An experimental investigation at 1 kbar, 800 °C and 0.5 kbar, 850 °C. Contributions to Mineralogy and Petrology, 121, 388–399.
Wolf, M.B., and London, D. (1994) Apatite dissolution into peraluminous haplogranite melt: An experimental study of solubilities and mechanisms. Geochimica et Cosmochimica Acta, 58, 4127–4145.
——— (1995) Incongruent dissolution of REE-and Sr-rich apatite in peraluminous granitic liquids: differential apatite, monazite, and xenotime solublities during anatexis. American Mineralogist, 80, 765–775.
Xie, J.C. (2008) The diagenesis and metallogenesis research of Mesozoic magmatic rocks in Tongling region, Anhui Province. Ph.D. thesis, University of Science and Technology of China (in Chinese with English abstract).
Xie, J., Yang, X., Sun, W., and Du, J. (2012) Early Cretaceous dioritic rocks in the Tongling region, eastern China: Implications for the tectonic settings. Lithos, 150, 49–61.
Xu, J.F., Shinjo, R., Defant, M.J., Wang, Q., and Rapp, R.P. (2002) Origin of Mesozoic adakitic intrusive rocks in the Ningzhen area of east China: partial melting of delaminated lower continental crust. Geology, 30, 1111–1114.
Xu, X.C., Lu, S.M., Xie, Q.Q., Bo, L., and Chu, G.Z. (2008a) SHRIMP zircon U-Pb dating for the magmatic rocks in Shizishan ore-field of Tongling, Anhui Province, and its geological implications. Acta Geologica Sinica, 82, 501–509 (in Chinese with English abstract).
Xu, X.C., Lu, S.M., Xie, Q.Q, Lou, J.W., and Chu, P.L. (2008b) Trace element geochemical characteristics of fluid inclusions of Dongguashan ore deposit in Tongling, Anhui Province, and their geological implications. Acta Petrologica Sinica, 24, 1865–1874.
Xu, L.L., Bi, X.W., Hu, R.Z., Tang, Y.Y., Wang, X.S., Huang, M.L., Wang, Y.J., Ma, R., and Liu, G. (2019) Contrasting whole-rock and mineral compositions of ore-bearing (Tongchang) and ore-barren (Shilicun) granitic plutons in SW China: Implications for petrogenesis and ore genesis. Lithos, 336-337, 54–66.
Yang, X.N., Xu, Z.W., Gao, G., Lu, X.C., Liu, S.M., and Li, H.Y. (2008) Fluid inclusion studies of the Chaoshan gold deposit in Tongling, Anhui Province, China. Acta Petrologica Sinica, 24, 1889–1899 (in Chinese with English abstract).
Yang, Y.H., Wu, F.Y., Yang, J.H., Chew, D.M., Xie, L.W., Chu, Z.Y., Zhang, Y.B., and Huang, C. (2014) Sr and Nd isotopic compositions of apatite reference materials used in U-Th-Pb geochronology. Chemical Geology, 385, 35–55.
Zajacz, Z., Candela, P.A., Piccoli, P.M., Wälle, M., and Sanchez-Valle, C. (2012) Gold and copper in volatile saturated mafic to intermediate magmas: Solubilities, partitioning, and implications for ore deposit formation. Geochimica et Cosmochimica Acta, 91, 140–159.
Zen, E. (1986) Aluminum enrichment in silicate melts by fractional crystallization: some mineralogic and petrographic constraints. Journal of Petrology, 27, 1095–1117.
Zhang, D., and Audétat, A. (2017) What caused the formation of the Giant Bingham Canyon porphyry Cu-Mo-Au deposit? Insights from melt inclusions and magmatic sulfides. Economic Geology, 112, 221–244.
Zhou, X.M., Sun, T., Shen, W.Z., Shu, L.S., and Niu, Y.L. (2006) Petrogenesis of Mesozoic granitoids and volcanic rocks in South China: A response to tectonic evolution. Episodes, 29, 26–33.
Zhu, J.J., Richards, J.P., Rees, C., Creaser, R., DuFrane, A., Locock, A., Petrus, J.A., and Lang, J. (2018) Elevated magmatic sulfur and chlorine contents in ore-forming magmas at the Red Chris Porphyry Cu-Au deposit, Northern British Columbia, Canada. Economic Geology, 113, 1047–1075.

Manuscript received February 26, 2020
Manuscript accepted December 17, 2020
Manuscript handled by Antonio Acosta-Vigil

Endnote:

[1]Deposit item AM-21-127497, Online Materials. Deposit items are free to all readers and found on the MSA website, via the specific issue's Table of Contents (go to http://www.minsocam.org/MSA/AmMin/TOC/2021/Dec2021_data/Dec2021_data.html).